

Dust Diffusion in Protoplanetary Discs by Magnetorotational Turbulence

Anders Johansen¹ and Hubert Klahr

Max-Planck-Institut für Astronomie, Königstuhl 17, 69117 Heidelberg, Germany

johansen@mpia.de

ABSTRACT

We measure the turbulent diffusion coefficient of dust grains embedded in magnetorotational turbulence in a protoplanetary disc directly from numerical simulations and compare it to the turbulent viscosity of the flow. The simulations are done in a local coordinate frame comoving with the gas in Keplerian rotation. Periodic boundary conditions are used in all directions, and vertical gravity is not applied to the gas. Using a two-fluid approach, small dust grains of various sizes (with friction times up to $\Omega_0 \tau_f = 0.02$) are allowed to move under the influence of friction with the turbulent gas. We measure the turbulent diffusion coefficient of the dust grains by applying an external sinusoidal force field acting in the vertical direction on the dust component only. This concentrates the dust around the mid-plane of the disc, and an equilibrium distribution of the dust density is achieved when the vertical settling is counteracted by the turbulent diffusion away from the mid-plane. Comparing with analytical expressions for the equilibrium concentration we deduce the vertical turbulent diffusion coefficient. The vertical diffusion coefficient is found to be lower than the turbulent viscosity and to have an associated vertical diffusion Prandtl number of about 1.5. A similar radial force field also allows us to measure the radial turbulent diffusion coefficient. We find a radial diffusion Prandtl number of about 0.85 and also find that the radial turbulent diffusion coefficient is around 70% higher than the vertical. As most angular momentum transport happens through magnetic Maxwell stresses, both the vertical and the radial diffusion coefficients are found to be significantly higher than suggested by the angular momentum transport by Reynolds stresses alone. We also find evidence for trapping of dust grains of intermediate friction time in turbulent eddies.

¹also at: NORDITA, Copenhagen, Denmark

Subject headings: diffusion — instabilities — MHD — planetary systems: protoplanetary disks — turbulence

\$Id: ms.tex,v 1.4 2005/08/17 07:59:04 ajohan Exp \$

1. INTRODUCTION

Knowledge of the transport properties of particles embedded in a turbulent gas medium is important in many aspects of protoplanetary disc modeling. If the spatial number density distribution of dust grains in a disc is required for the model, one must know the effect of turbulent diffusion on the dust grains.

Vertical diffusion — The distribution of tiny dust grains, with radii smaller than around 100 μm , determines the observability of protoplanetary discs around young stellar objects through their contribution to the infrared parts of the spectrum. An interesting observational effect of turbulent diffusion is its influence on the vertical settling of dust grains. The settling affects the spectral energy distribution of protoplanetary discs, since flaring discs, i.e. where the scale height of the gas density increases with radial distance, have a much stronger mid- to far-infrared excess than self-shadowing discs, where the scale height after a certain distance from the protostar begins to fall with radial distance (e.g. Dullemond 2002). Recent model calculations by Dullemond & Dominik (2004) show that the vertical settling of dust grains towards the mid-plane of the disc can change an initially flaring disc into a partially self-shadowing disc, thus effecting the observability of the disc. These calculations depend – among other things – on the strength of the turbulence in the disc (the turbulent viscosity) and on the turbulent diffusion coefficient of dust grains in the direction perpendicular to the disc mid-plane. Also, Ilgner et al. (2004) recently considered the effect of vertical mixing in protoplanetary discs on the distribution of various chemical species and found the distribution to be influenced greatly by mass transport processes, again underlining the importance of vertical turbulent diffusion in the modeling of protoplanetary discs.

Radial diffusion — Crystalline silicate dust grain features observed in comet spectra are often attributed to radial mixing in the solar nebula (e.g. Hanner 1999). Silicate dust grains are formed primarily in amorphous form, but they can become crystalline if exposed to temperatures above ~ 1000 K. Such a heating can obviously have occurred in the hot inner parts of the solar nebula, whereas comets are expected to have formed in the cold outer regions of the nebula, so in this picture some radial mixing must take place between the inner

and outer nebula. Bockelée-Morvan et al. (2002) consider disc models where crystallization of silicates happens in the inner, hot parts of the disc. They calculate that in a few times 10^4 years the crystalline silicate fraction reaches a uniform value outside the crystallization region due to radial turbulent diffusion, and that the value can approach unity for realistic disc parameters. From high resolution observations of three protoplanetary discs, van Boekel et al. (2004) find that the inner 1-2 AU of these discs contain a higher crystalline silicate fraction than the outer 2-20 AU. This supports the theory that crystalline dust grains form in the hot inner disc and are subsequently transported to the outer disc by turbulent gas motion.

The existence of chondrules (millimeter-sized solid inclusions found in primitive meteorites, see e.g. Norton 2002) is believed to be the result of collisions and coagulation of small dust grains (Blum & Wurm 2000). The size distribution of chondrules may be explained by selective sorting in the turbulent solar nebula (Cuzzi et al. 2001). The first step in planet formation is the build-up of kilometer-sized rocky and icy planetesimals (in the planetesimal hypothesis of Safronov 1969), either from sticking or due to a gravitational instability in the vertically settled dust layer. In the latter case, the equilibrium scale height of the dust layer is determined by the turbulent diffusion coefficient of the dust grains in the vertical direction (Cuzzi et al. 1993). An alternative planet formation hypothesis, the gravitational instability hypothesis (see Boss 2003, and references therein), states that planets form as a direct gravitational instability in the gas of a protoplanetary disc. The ability of a disc to undergo gravitational instability depends on its density and temperature structure, which is again dependent on the distribution and thus the turbulent transport of tiny dust grains.

It is a modern paradigm of protoplanetary discs that shear instabilities in the gas flow lead to turbulence, which is again responsible for such diverse effects as heating, angular momentum transport and diffusion. The actual turbulence is often parametrized in a single parameter, the turbulent viscosity (which can be non-dimensionalized into the α -value of Shakura & Sunyaev 1973). This single parameter determines both heating, angular momentum transport and diffusion. Candidates for protoplanetary disc turbulence are many. Most pronounced linear instabilities are vertical convective instability (Lin & Papaloizou 1980) and the magnetorotational instability (Balbus & Hawley 1991), although the former has proved to lead to inward rather than outward transport of angular momentum (Ryu & Goodman 1992). Other instabilities have been proposed, such as the baroclinic instability of Klahr & Bodenheimer (2003) which must be non-linear according to Klahr (2004), a linear Rossby wave instability (Li et al. 2000) and a linear stratorotational instability (Dubrulle et al. 2005; Shalybkov & Rüdiger 2005).

Today's most accepted source of turbulence is magnetorotational turbulence (MRI).

For completely ionized discs, the emergence of self-sustained turbulence through the linear magnetorotational shear instability seems inevitable, both in local shearing box simulations (Brandenburg et al. 1995; Hawley et al. 1995) and in global accretion disc simulations (Armitage 1998; Arlt & Rüdiger 2001). The application of the ideal MHD equations to protoplanetary discs is only justified where the ionization fraction is relatively high (e.g. Fromang et al. 2002; Semenov et al. 2004). This may be given in the hot and dust-free inner parts of the disc, as well as away from the mid-plane of the disc and at large radial distances where the ionization is determined by cosmic ray and high energy photon penetration. In protoplanetary discs this had lead to the concept of a magnetically dead zone near the mid-plane of the disc where the ionization fraction is too low to sustain MRI. Fleming & Stone (2003) consider local shearing box simulations with a vertically dependent ionization fraction and find that some turbulent stresses are induced in the dead zone by the surrounding MRI turbulence. Thus angular momentum can be transported even in regions of the disc that are not magnetorotationally unstable.

It is often assumed that turbulent transport takes place as diffusion. For dust grains, the turbulent flux is assumed proportional to the gradient of the dust-to-gas ratio (Dubrulle et al. 1995). Such a prescription does not per se determine a certain value for the turbulent diffusion coefficient. Hence it is often parametrized to be a scalar that is equal to the turbulent viscosity of the gas for tiny grains but falls gradually for larger and larger grain sizes (Cuzzi et al. 1993; Schröppler & Henning 2004). One argument for setting the turbulent diffusion coefficient equal to the turbulent viscosity is that the radial velocity fluctuations are the base of both (non-magnetic) angular momentum transport and diffusion (Tennekes & Lumley 1972, p. 143). Such an approach is simple to use, but caution should be taken regarding its validity, both regarding the numerical value of the turbulent diffusion coefficient and regarding the isotropy that is implicitly assumed when making it a scalar.

The validity of the whole diffusion description must also be addressed. An obvious cause of concern is the presence of dust-trapping mechanisms in the turbulent gas flow. Gas turbulence and global pressure gradients, e.g. from vertical and radial stratification, are the cause of two important trapping mechanisms. Whenever the gas is pressure-supported and in force balance, the embedded dust grains feel an excess force in the opposite direction to the gas pressure gradient, since they can never be in the same force equilibrium without pressure support. The dust grains thus feel an acceleration relative to the gas. This has various effects, e.g. vertical settling of the dust layer towards the mid-plane of protoplanetary discs or inward radial drift of dust grains if there is an outwards decreasing gas pressure in the disc, a notorious problem in planet formation (Weidenschilling 1977). The dust grains reach a terminal velocity when the friction with the gas balances out the acceleration due to the missing pressure gradient. The terminal velocity of very small dust grains is proportional to

the friction time. In non-turbulent disc models only global pressure gradients are present, but in a turbulent disc local, fluctuating regions of high and low pressure are expected to occur. Then dust grains continuously move up the local pressure gradient, and this contributes to the random motion of the grains, which is responsible for turbulent diffusion. Magnetic pressure gradients actually give the same effect, as we will show analytically in Sect. 2.3. A local concentration of dust grains can not be described as diffusion, so one of the goals of this paper is to test the validity of the global diffusion picture in the presence of turbulent pressure gradient trapping.

For larger dust grains, where the friction time becomes comparable to the orbital period of the disc, another important dust-trapping mechanism sets in. Stationary rotational structures in the gas (e.g. anticyclones) are given by an equilibrium between the global Coriolis force from the rotating disc and the centrifugal force of the rotating structure. As they enter such a structure, large dust grains experience a slow acceleration, due to drag forces with the gas. Rotating initially with the gas, but much slower, the Coriolis force dominates over the centrifugal force, and the dust grains are sucked into the eddy. This vortex trapping was proposed by Barge & Sommeria (1995), and has since then been subject of much theoretical investigation (e.g. Chavanis 2000; Johansen et al. 2004). The conclusions are that vortices are extremely efficient at trapping dust grains, and this efficiency may even explain how gas planets are formed before the dispersion of the gas disc (Klahr & Bodenheimer 2005). Vortex trapping would seem to be potentially even more threatening to the global diffusion description than pressure gradient trapping.

In this paper we measure the turbulent diffusion coefficient of dust grains directly from numerical simulations of three-dimensional magnetorotational turbulence. We treat the physics of protoplanetary discs in the shearing sheet approximation, in which a local coordinate frame corotating with the disc is considered. Dust is added as an extra fluid that interacts with the gas through a drag force. The turbulent diffusion coefficient is measured by exposing the dust fluid to an external force field and then comparing the resulting dust density with analytical expressions derived with a parametrized diffusion term. By comparing the measured value to the turbulent viscosity we examine whether the two are indeed equal as is often assumed. We specifically address the question of whether the diffusion coefficient is isotropic by measuring diffusion in both the vertical and the radial direction. Finally we quantify the effect of dust-trapping mechanisms on the whole diffusion picture by examining correlations between turbulent gas features and the dust-to-gas ratio.

The paper is built up as follows. In Sect. 2 we describe the dynamical equations for the motion of gas and dust and the computer code that we use to solve them numerically. Then we go into details in Sect. 3 about how we deduce the turbulent diffusion coefficient from

computer simulations by comparing the equilibrium dust density with analytical expressions. In Sect. 4 we describe the units and the boundary conditions of the simulations. The results are described in the following two sections; Sect. 5 describes the turbulent evolution of the gas while Sect. 6 describes the evolution of the dust, especially the measured turbulent diffusion coefficients and diffusion Prandtl numbers and the presence of dust-trapping mechanisms in the gas. Finally conclusions, discussions and some outlook to potential further investigations into the subject of turbulent diffusion of dust grains appear in Sect. 7.

2. DYNAMICAL EQUATIONS

In this section we present the dynamical equations we use for gas velocity, gas density, magnetic vector potential, dust velocity and dust density. We integrate the dynamical equations using the Pencil Code¹. This is a finite difference code that uses sixth order centered spatial derivatives and a third order Runge-Kutta time-stepping scheme. See Brandenburg (2003) for details on the numerical schemes and test runs. The Pencil Code solves the dynamical equations in their non-conservative form and gives very similar results to the ZEUS code for the statistical properties of MRI turbulence (see Balbus & Hawley 1998, and references therein).

The Pencil Code requires artificial diffusivity terms in the dynamical equations to stabilize the finite difference numerical scheme. For the purpose of calculating turbulent diffusion coefficients it is vital that we can reduce the artificial mass diffusion as much as possible in order to distinguish the measured turbulent diffusion from the imposed artificial diffusion. The biggest contribution to the turbulent transport of dust grains is expected to come from the fast and far moving large scales, so keeping the large scales unaffected by diffusion is important. To achieve this we use hyperdiffusivity terms in all the dynamical equations. Hyperdiffusivity involves replacing the regular diffusivity terms (involving second order derivatives) with differential operators that use higher order derivatives. This quenches unstable modes at the smallest scales of the simulation, while at the same time the large scales are kept unaffected by diffusivity. We have checked, by varying the value of the artificial diffusion coefficient, that hyperdiffusion does not have any effect on the turbulent diffusion coefficients that we measure. The use of hyperdiffusivity is discussed further in Appendix A. There the hyperversions that we adopt for viscosity, mass diffusion and resistivity are also presented.

¹The code is available at
<http://www.nordita.dk/software/pencil-code>

In this section we also develop a method for being able to treat numerically the motion of very tiny dust grains with friction times much shorter than the computational time-step of the gas. This so-called short friction time approximation is presented and discussed in the last part of the section.

2.1. Gas Dynamics

We consider the motion of gas and dust in the shearing sheet approximation (e.g. Goldreich & Tremaine 1978; Brandenburg et al. 1995). Here a local coordinate frame corotating with the disc at a distance r_0 from the central source of gravity is considered. The coordinate axes are defined as following. The x -axis points always away from the central gravity source, and the y -axis points in the direction of the Keplerian flow (as seen from a non-comoving frame). The z -axis points perpendicular to the disc along the direction of the angular velocity vector $\boldsymbol{\Omega}_0$ of the orbital motion. In this frame, the Keplerian flow velocity field has the linearized form $\mathbf{u}_0 = -\frac{3}{2}\Omega_0 x \hat{\mathbf{y}} \equiv u_y^{(0)} \hat{\mathbf{y}}$. We choose to measure velocities relative to the Keplerian flow, $\mathbf{u} - \mathbf{u}_0 \rightarrow \mathbf{u}$. Such a transformation introduces new shear terms in the equation of motion, but it has the advantage that the Keplerian velocity is zero everywhere. The equation of motion relative to the main shear flow in the shearing sheet approximation is

$$\frac{\partial \mathbf{u}}{\partial t} = -(\mathbf{u} \cdot \nabla) \mathbf{u} - u_y^{(0)} \frac{\partial \mathbf{u}}{\partial y} + \mathbf{f}(\mathbf{u}) - \frac{1}{\rho} \nabla P + \frac{1}{\rho} \mathbf{J} \times \mathbf{B} + \mathbf{f}_\nu(\mathbf{u}, \rho). \quad (1)$$

The first term on the right hand side of equation (1) is the advection due to any velocity relative to the main shear flow, while the second term covers the advection due to the shear flow. The function $\mathbf{f}(\mathbf{u})$ is defined as

$$\mathbf{f}(\mathbf{u}) = \begin{pmatrix} 2\Omega_0 u_y \\ -\frac{1}{2}\Omega_0 u_x \\ 0 \end{pmatrix} \quad (2)$$

and is an effect of Coriolis force. The last three terms in equation (1) are the pressure gradient force, the magnetic Lorentz force (where the volume current density \mathbf{J} is defined through Ampère’s law $\nabla \times \mathbf{B} = \mu_0 \mathbf{J}$), and a hyperviscosity term based on the function \mathbf{f}_ν defined in equation (A4). We ignore the effect of vertical gravity on the gas, because we are interested in the ideal case to measure the isotropy/non-isotropy of magnetorotational turbulence and the local transport properties of the gas without introducing additional isotropy-breaking effects. Ignoring the stratification effectively means that we are considering the disc close to the mid-plane where the vertical gravity is vanishing. Future work on the properties of dust diffusion in local shearing box simulations should take the vertical stratification of the disc into account.

The evolution of the gas density ρ is determined by the continuity equation

$$\frac{\partial \rho}{\partial t} = -u_y^{(0)} \frac{\partial \rho}{\partial y} - \rho \nabla \cdot \mathbf{u} - \mathbf{u} \cdot \nabla \rho + f_D(\rho), \quad (3)$$

where the first term on the right hand side is again an effect of advection due to the main shear flow. The two next terms come from the standard term $\nabla \cdot (\rho \mathbf{u})$ from the continuity equation. In the last term we include artificial mass diffusion through the function f_D defined in equation (A6). An isothermal equation of state is used where the pressure depends on the density as $P = c_s^2 \rho$. Here c_s is the constant sound speed.

The induction equation determines the evolution of the magnetic vector potential \mathbf{A} . Evolving the vector potential has the advantage over evolving the magnetic field $\mathbf{B} = \nabla \times \mathbf{A}$ in that it maintains a solenoidal magnetic field (i.e. $\nabla \cdot \mathbf{B} = 0$) at all times. The induction equation in the shearing sheet approximation is

$$\frac{\partial \mathbf{A}}{\partial t} = -u_y^{(0)} \frac{\partial \mathbf{A}}{\partial y} + \frac{3}{2} \Omega_0 A_y \hat{\mathbf{x}} + \mathbf{u} \times \mathbf{B} + \mathbf{f}_\eta(\mathbf{A}). \quad (4)$$

The first term on the right hand side of equation (4) is the advection due to the main shear flow, while the second is the so-called magnetic stretching term, another effect of shear (Brandenburg et al. 1995). The two last terms are the standard electromotive force and a resistivity term based on the function \mathbf{f}_η defined in equation (A8).

2.2. Dust Dynamics

The dust grains are considered as a fluid without any pressure support. Any pressure gradient force on the dust due to collisions between dust grains and gas molecules can also be ignored since the solid density of dust grains is so large that the resulting acceleration is negligibly small.

In the fluid approach, the equation of motion for the dust velocity relative to the Keplerian flow is

$$\frac{\partial \mathbf{w}}{\partial t} = -(\mathbf{w} \cdot \nabla) \mathbf{w} - u_y^{(0)} \frac{\partial \mathbf{w}}{\partial y} + \mathbf{f}(\mathbf{w}) + \mathbf{f}_\nu(\mathbf{w}, n) - \frac{1}{\tau_f} (\mathbf{w} - \mathbf{u}) + \mathbf{g}(x, y, z). \quad (5)$$

The first four terms on the right hand side appear similar here as in the gas momentum equation. The last two terms in equation (5) are the drag force and an externally imposed force field \mathbf{g} that we use to drive a non-zero diffusion equilibrium in the dust density. This is explained in more detail in Sect. 3.

We let the dust and the gas couple through a drag force proportional to, but in the opposite direction of, the velocity difference between the dust and the gas. The strength of the drag force is characterized by the friction time τ_f . Any relative motion between dust and gas is damped by the drag force with an e-folding time of τ_f . The physics of the dust grain and the gas enters in the expression of the friction time. When the mean free path of the gas molecules is larger than the dust grain radius, the dust grain is in the Epstein regime (e.g. Weidenschilling 1977). Here the friction time of a spherical dust grain with radius a_\bullet and solid density ρ_\bullet can be expressed as

$$\tau_f = \frac{a_\bullet \rho_\bullet}{c_s \rho}, \quad (6)$$

where c_s is the sound speed in the surrounding gas and ρ is the gas density. The sound speed and the gas density are approximately constant in the unstratified and isothermal case, so we can treat τ_f as constant that depends only on the given particle radius and solid density.

Treating dust as a fluid is justified as long as the mean free path of the fluid constituents is smaller than the typical dimensions of the system. In the case of the gas, one compares the mean free path of the molecules with the thickness of the disc H_0 . For the dust grains the collisions among the grains themselves are unimportant for determining a mean free path. Here the collisions with the gas molecules are the important effect. The mean free path for the dust grains can be defined as the distance one grain has to float with respect to the gas before it has lost a significant fraction of its momentum. For a spherical grain moving with a speed w relative to the gas, this value can be determined as $\ell = w\tau_f$. The condition for treating dust as a fluid is then that $\ell \ll H_0$. Because all motions are subsonic, we can replace w by c_s as an upper limit and get the expression $\Omega_0\tau_f \ll 1$ for the validity of the fluid approach.

In a typical solar nebula type protoplanetary disc, the scale height is of the order of $H_0 \sim 10^{12}$ cm at $r_0 = 5$ AU, while the gas density can be taken to $\rho_0 \sim 10^{-10}$ g cm $^{-3}$ at the same radial distance. Then the connection between grain radius and dimensionless friction time is

$$a_\bullet = \Omega_0\tau_f H_0 \frac{\rho_0}{\rho_\bullet} \sim 10^2 \Omega_0\tau_f \text{ cm}. \quad (7)$$

This means that, as a rule of thumb, the value of the dimensionless friction time corresponds to the radius of the dust grain measured in meters.

To preserve momentum the gas should be affected by a drag force $\mathbf{f}_{\text{drag}} = -\tau_f^{-1} \rho_d / \rho (\mathbf{u} - \mathbf{w})$ from the dust. Here ρ_d / ρ is the dust-to-gas ratio. We shall ignore the back-reaction drag force from the dust on the gas, because the dust-to-gas ratio is small in the early stages of a protoplanetary disc.

We represent dust mass density by the number density n of dust grains. The continuity equation for the dust number density n is

$$\frac{\partial n}{\partial t} = -u_y^{(0)} \frac{\partial n}{\partial y} - n \nabla \cdot \mathbf{w} - \mathbf{w} \cdot \nabla n + f_D(n), \quad (8)$$

where we use artificial diffusion, through the function $f_D(n)$ defined in equation (A6), only to stabilize the numerical scheme. By varying the value of the artificial diffusion coefficient D_3 , which is defined in Appendix A, we have made sure that adding artificial diffusion has no effect on the measured turbulent diffusion coefficients. The value of D_3 needed to stabilize the runs are for all runs several orders of magnitude below the measured turbulent diffusion coefficient.

We now have two possibilities to solve the dust equation of motion (eq. [5]): For large particles, with friction times larger than the Courant time-step ($\Omega_0 \tau_f > 0.001$, see Table 1), we can use the explicit integration scheme from the Pencil Code. But for the smaller particle cases ($\Omega_0 \tau_f \ll 0.001$), where the friction time is much shorter than the Courant time-step, we will use the short friction time approximation, a semianalytical time integration that is presented below.

2.3. Short Friction Time Approximation

The radii of dust grains observed in protoplanetary discs are often on the order of micrometers or even nanometers. The friction time of microscopic dust grains in a protoplanetary disc is very short compared to the orbital period, around a few minutes for the location of Jupiter in a typical solar nebula. That is of course not a problem for nature, but the smallest scales of computer simulations are many orders of magnitude larger than in nature, and thus the computational time-step for an explicit code such as the Pencil Code is much larger than the friction time of tiny dust grains. This causes a potential problem in resolving both timescales at the same time. To follow the motion of the tiniest dust grains, applying the explicit integration scheme as used in the Pencil Code, a time-step must be chosen that is at least an order of magnitude shorter than the friction time. Thus the computation time for simultaneously following the evolution of gas and dust becomes prohibitively long. One can now either use an implicit integration scheme, which would introduce further problems, and also make major changes in the code necessary, or one can use a kind of semianalytical integration scheme that works as follows.

For very short friction times, the dust is able to settle to an equilibrium velocity, where the drag force is exactly balanced by the other force terms that are present in the dust

equation of motion (eq. [5]), on a timescale that is much shorter than the computational time-step of the gas. Thus it is possible, under a few reasonable assumptions, to solve algebraically for the terminal dust velocity as a function of gas velocity and density. To do this, we first subtract the gas equation of motion (eq. [1]) from the dust equation of motion (eq. [5]). This results in an equation for the evolution of relative velocity $\mathbf{w} - \mathbf{u}$,

$$\frac{\partial(\mathbf{w} - \mathbf{u})}{\partial t} + (\mathbf{w} \cdot \nabla)\mathbf{w} - (\mathbf{u} \cdot \nabla)\mathbf{u} + u_y^{(0)} \frac{\partial(\mathbf{w} - \mathbf{u})}{\partial y} = \mathbf{f}(\mathbf{w} - \mathbf{u}) - \frac{1}{\tau_f}(\mathbf{w} - \mathbf{u}) + \mathbf{g} + \frac{1}{\rho}(\nabla P - \mathbf{J} \times \mathbf{B}), \quad (9)$$

where the viscosity terms have been ignored since any real physical viscosity is expected to be orders of magnitude weaker than the other force terms. We now assume that the computational time-step of the gas is much longer than the friction time, $\delta t \gg \tau_f$. Here δt will be given by the Courant criterion. This criterion determines the maximum time-step that can be taken by an explicit numerical scheme without becoming unstable. The allowed time-step gets shorter with increasing grid resolution. With the condition $\delta t \gg \tau_f$, all terms from the gas equation of motion can be considered to be constant for the duration of the acceleration of the dust grain to its terminal velocity. This specifically also applies to the pressure gradient force and the Lorentz force that are present also in equation (9). Then we can search for a time-independent equilibrium solution for $\mathbf{w} - \mathbf{u}$. We expect any time-independent solution of equation (9) to have a dust velocity that is very close to the gas velocity, because the short friction time couples the dust velocity strongly to the gas velocity. Setting therefore $\mathbf{w} = \mathbf{u}$ in all other terms than the drag force term (this is legitimized below) leaves the algebraic equilibrium equation

$$0 = -\frac{1}{\tau_f}(\mathbf{w} - \mathbf{u}) + \mathbf{g} + \frac{1}{\rho}(\nabla P - \mathbf{J} \times \mathbf{B}). \quad (10)$$

Solving for \mathbf{w} then yields

$$\mathbf{w} = \mathbf{u} + \tau_f \left[\mathbf{g} + \frac{1}{\rho}(\nabla P - \mathbf{J} \times \mathbf{B}) \right]. \quad (11)$$

Reinserting this solution into equation (9) shows that it was reasonable to ignore all advection, shear and Coriolis terms, while keeping the friction, gravity, pressure gradient and Lorentz terms, as long as the friction time is sufficiently short.

This is the short friction time approximation. The specific form of the short friction time dust velocity approximation depends on the forces that are assumed to work on the gas and on the dust, so equation (11) is only valid for the specific choice of force terms that are considered in this work. The presence of gravity in the dust velocity approximation comes from only considering gravity to work on the dust. This is good for the purpose of measuring the turbulent diffusion coefficient, whereas in nature gravity of course affects both

dust and gas. The gravity term would then drop out of the short friction time approximation, but it would reappear in the form of the vertical pressure gradient of the stratified gas. One must also take into consideration that the dust velocity in equation (11) is expressed as a function of the resolved part of the gas velocity only. All unresolved small scales would also contribute to the random motion of the tiny dust grains (as would Brownian motion), but the important scales for turbulent transport are the largest scales in the box, since they contribute most to the total gas velocity field.

The equilibrium dust velocity given by the short friction time approximation ensures that the relative velocity between dust and gas does not change on timescales shorter than the computational time-step. That means that if the gas is being accelerated, then the same amount of acceleration must be working on the dust, and so the relative velocity between the dust and the gas stays constant until sufficient time has passed for the pressure gradient force and the Lorentz force to change at the computational timescale.

The i th component of the Lorentz force appearing in equation (11) can be rewritten as

$$(\mathbf{J} \times \mathbf{B})_i = \nabla_j \left(\frac{B_i B_j}{\mu_0} - \frac{B^2}{2\mu_0} \delta_{ij} \right), \quad (12)$$

where the first term in the parenthesis on the right hand side is due to magnetic pressure and the second to magnetic tension. This allows the i th component of the short friction time approximation dust velocity to be rewritten as

$$w_i = u_i + \tau_f \left[g_i + \frac{1}{\rho} \nabla_j \left(P \delta_{ij} + \frac{B^2}{2\mu_0} \delta_{ij} - \frac{B_i B_j}{\mu_0} \right) \right]. \quad (13)$$

Thus dust grains move relative to the gas not only because of (additional) gravity and (missing) pressure gradient force, but also due to (missing) magnetic pressure gradient force and (missing) magnetic tension. We shall still refer to the effect as pressure gradient trapping, even though the magnetic tension term in equation (13) does not mimic a pressure gradient.

We must stress again that the short friction time approximation is only valid for small particles. If one considers larger bodies (e.g. > 1 mm at $r_0 = 5$ AU in a typical solar nebula), first the Coriolis forces and then the advective transport terms can no longer be ignored. For these particles we directly integrate the dust equation of motion (eq. [5]) together with the other dynamical equations. With even larger objects finally the fluid approach fails as soon as $\ell > H_0$. In this case one has to apply a particle algorithm to follow the dust evolution (e.g. Klahr & Henning 1997).

3. DIFFUSION COEFFICIENT

In this section we describe how we calculate the diffusion coefficient of dust grains embedded in a turbulent gas. We do this by comparing the results of numerical simulations with analytical solutions to the non-turbulent flow equations that include a parametrized diffusion.

If the turbulent motion of the gas and the dust has not been resolved, the continuity equation of the dust would have to incorporate an explicit diffusion term,

$$\frac{\partial n}{\partial t} = -\nabla \cdot \left[(\mathbf{w} + u_y^{(0)} \hat{\mathbf{y}})n - D_t \rho \nabla \left(\frac{n}{\rho} \right) \right]. \quad (14)$$

The gas flow is here assumed to be completely stationary, and the only effect of the non-resolved turbulence is through the parametrized diffusion term. The continuity equation is written in a conservative form where the diffusion flux is proportional to and in the opposite direction of the gradient of the dust-to-gas ratio. This is the way turbulent diffusion is normally assumed to act (see e.g. Dubrulle et al. 1995).

The task now is to find a way to extract D_t from the non-stationary turbulent motion found in computer simulations. This is only possible if ∇n is not zero everywhere, as otherwise the diffusion coefficient does not enter equation (14) at all for a constant ρ . One can now either follow the time dependent diffusion of an initial dust concentration somewhere in the center of the box or look for a time independent equilibrium solution. The first approach has the disadvantage that it is difficult to obtain good statistics, as one has always a very special distribution with a distinct wavelength, whereas the turbulence could act on all scales. Therefore we use the latter possibility and search for an equilibrium solution where we can achieve much better statistics.

We force an equilibrium solution with a non-zero dust density gradient by exposing the grains to an external force field \mathbf{g} . Depending on its specific form, this force field will eventually result in an equilibrium where the pile-up of dust grains imposed by \mathbf{g} is balanced completely by mass diffusion in the opposite direction. By comparing the analytical expression for the equilibrium dust number density, whose only free parameter is D_t , to the equilibrium density obtained when the turbulence is resolved in computer simulations, we can derive the turbulent diffusion coefficient. We will often refer to the external force field simply as gravity because of the qualitative similarities to real gravity.

First the diffusion in the z -direction is considered. Here we define a vertical gravity field

$$g_z = -g_0 \sin(k_z z), \quad (15)$$

where $k_z = 2\pi/L_z$ in order to have periodic boundaries in the vertical direction. Here L_z is the vertical extent of the box, and z is defined to lie in the interval between $-\frac{1}{2}L_z$ and $\frac{1}{2}L_z$. Using periodic boundary conditions demands that we use a periodic force field in order to have a periodic equilibrium solution. The gravity field defined in equation (15) is linear around the mid-plane, as the gravity field normally considered for thin discs also is, but away from the mid-plane it becomes zero again on the top and bottom boundaries of the box. Such a force gives a periodic dust distribution to determine the turbulent viscosity coefficient from (we will show below that the equilibrium logarithmic dust density becomes cosinusoidal with z). For a normal thin disc vertical gravity field, $g_z = -\Omega_0^2 z$, the equilibrium logarithmic dust density becomes quadratic with z , which is obviously not periodic.

To find the equilibrium dust number density, we solve now equations (5) and (14) for $\partial \mathbf{w}/\partial t = \partial n/\partial t = \mathbf{u} = w_x = w_y = 0$, $w_z = w_z(z)$ and $n = n(z)$. This yields the differential equation system

$$0 = -w_z \frac{\partial w_z}{\partial z} - \frac{1}{\tau_f} w_z - g_0 \sin(k_z z), \quad (16)$$

$$0 = -\frac{\partial}{\partial z} \left(w_z n - D_z^{(t)} \frac{\partial n}{\partial z} \right), \quad (17)$$

where we neglect the ρ -dependence in the diffusion term, because the turbulent gas density fluctuations are very small, as expected in subsonic turbulence. For any sufficiently short friction time, the advection term in equation (16) can be safely ignored, leaving only the algebraic equation

$$0 = -\frac{1}{\tau_f} w_z - g_0 \sin(k_z z) \quad (18)$$

with the solution

$$w_z = -\tau_f g_0 \sin(k_z z). \quad (19)$$

Inserting equation (19) into equation (16) shows that the advection term is fully negligible for $\tau_f^2 g_0 k_z \ll 1$.

The equilibrium solution to the continuity equation must now be able to continuously replace material that is being transported towards the mid-plane by new material transported away from the mid-plane by diffusion. It is seen that equation (17) has the general solution

$$\ln n = \frac{1}{D_z^{(t)}} \int w_z(z) dz \quad (20)$$

for any integrable function $w_z(z)$. Here we have assumed that there is no net flux of dust grains $\overline{w_z} = 0$ by setting the contents of the parenthesis on the right hand side of equation

(17) equal to zero. Inserting the equilibrium dust velocity from equation (19) into the integral in equation (20) gives the equilibrium logarithmic dust number density as

$$\ln n = \ln n_1 + \frac{\tau_f g_0}{k_z D_z^{(t)}} \cos(k_z z), \quad (21)$$

where $\ln n_1$ is an integration constant that corresponds physically to the logarithmic number density at $z = \pm \frac{1}{4} L_z$. The amplitude of the cosine distribution depends only on friction time, gravity strength and gravity wave number, which are all known input parameters, and the unknown value of the turbulent diffusion coefficient in the vertical direction. Thus the value of the turbulent diffusion coefficient can be determined uniquely from this amplitude.

The number density distribution in equation (21) is not normalized. The connection between n_1 and the column density Σ_0 is

$$\Sigma_0 = \int_{-1/2 L_z}^{1/2 L_z} n_1 \exp \left[\frac{\tau_f g_0}{k_z D_z^{(t)}} \cos(k_z z) \right] dz = \frac{2\pi n_1}{k_z} \frac{1}{\pi} \int_0^\pi \exp \left[\frac{\tau_f g_0}{k_z D_z^{(t)}} \cos(k_z z) \right] d(k_z z), \quad (22)$$

where the last equality holds because the cosine function is symmetric in z . The modified Bessel function of the first kind of order m is defined as

$$I_m(x) = \frac{1}{\pi} \int_0^\pi e^{x \cos \theta} \cos(m\theta) d\theta, \quad (23)$$

so the connection between Σ_0 and n_1 becomes simply

$$\Sigma_0 = \frac{2\pi n_1}{k_z} I_0 \left(\frac{\tau_f g_0}{k_z D_z^{(t)}} \right). \quad (24)$$

Isolating n_1 finally yields

$$n_1 = \frac{k_z \Sigma_0}{2\pi I_0 \left(\frac{\tau_f g_0}{k_z D_z^{(t)}} \right)}. \quad (25)$$

For infinite diffusion $D_z^{(t)} \rightarrow \infty$, the argument of the Bessel function in equation (25) is zero, and using $I_0(0) = 1$ from equation (23), we get $\Sigma_0 = n_1 L_z$. Thus $n_1 = n_0$, where n_0 is the average dust number density in the box, as expected for the special case of infinite diffusion. In the case of a finite diffusion coefficient, $n_1 \neq n_0$.

For the radial x -direction, a similar sinusoidal gravity field can be defined to give the equilibrium dust density as

$$\ln n = \ln n_1 + \frac{\tau_f g_0}{k_x D_x^{(t)}} \cos(k_x x), \quad (26)$$

formally identical to the vertical case. The derivations are given in Appendix B. With equations (21) and (26) we are armed with two powerful analytical expressions for the number

density distribution of dust grains in diffusion equilibrium with an externally imposed force field. By comparing computer simulations of magnetorotational turbulence with these analytical results, we can extract the turbulent diffusion coefficient of the dust grains in both the vertical and the radial directions independently. The next sections describe the setup of the simulations and the results that we get.

4. UNITS AND BOUNDARY CONDITIONS

We adopt non-dimensional variables by measuring velocities relative to the isothermal sound speed, $[\mathbf{u}] = [\mathbf{w}] = c_s$, and densities relative to the initial density in the box, $[\rho] = \rho_0$; $[n] = n_0$. The unit of dust-to-gas ratio ϵ_d is $[\epsilon_d] = \epsilon_0 = m_0 n_0 / \rho_0$, where m_0 is the mass of the individual dust grains. Time is measured in units of inverse Keplerian angular speed, $[t] = \Omega_0^{-1}$, although often stated in orbits $T = 2\pi\Omega_0^{-1}$. The unit of magnetic field is $[\mathbf{B}] = c_s \sqrt{\mu_0 \rho_0}$. Derived from these basic units are the unit of distance $[\mathbf{x}] = c_s \Omega_0^{-1}$ and the unit of magnetic vector potential $[\mathbf{A}] = c_s^2 \Omega_0^{-1} \sqrt{\mu_0 \rho_0}$. The unit of turbulent viscosity and turbulent diffusion coefficient can also be derived from the basic units to be $[\nu_t] = [D_t] = c_s^2 \Omega_0^{-1}$. In these units the turbulent viscosity and the turbulent α -value take the same numerical value.

We choose a box length of 2π in all directions. In order to keep the background shear flow subsonic at all points we choose the arbitrary normalization $\Omega_0 = 0.2$. We have checked by setting Ω_0 to unity that the evolution of the simulations indeed scale with the value of Ω_0 , and thus that the scale-free diffusion coefficients and α -values are independent of the choice of Ω_0 .

Periodic boundary conditions are applied in all directions. Connected points at the periodic x -boundary have a time-dependent shift as is appropriate in the shearing sheet approximation.

5. EVOLUTION OF GAS

As an initial condition, we perturb the gas velocity components with random fluctuations of amplitude $\delta\mathbf{u} \sim 10^{-3}$. The toroidal component of the magnetic vector potential is perturbed by a standing cosine wave $A_y = A_0 \cos(k_x x) \cos(k_y y) \cos(k_z z)$ of amplitude $A_0 = 0.2$ and wave numbers $k_x = k_y = k_z = 1$. The resulting vertical component of the magnetic field is $B_z = -A_0 k_x \sin(k_x x) \cos(k_y y) \cos(k_z z) = B_0(x, y) \cos(k_z z)$. Such a wave is unstable to shear if k_z is sufficiently small (i.e. at sufficiently large scales). As shown by Balbus & Hawley (1991), the wave number interval for instability of the vertical magnetic

field component is $0 < k_z < \sqrt{3}\Omega_0/v_A$, where the Alfvén speed is defined as $v_A^2 = B_0^2/(\mu_0\rho_0)$. For $0 < |B_0| < 0.2$, the upper limit wave number is always larger than around $k_z = \sqrt{3}$, so $k_z = 1$, the largest scale present in the simulation, is well within the unstable regime.

We run simulations in two different resolutions, 64^3 and 128^3 . In Table 1 the parameters that are used in the different runs are listed. As there is no back-coupling from the dust on the gas, the gas evolution depends mainly on resolution, since the high resolution runs require less artificial diffusivity. The dust only affects the gas through its contribution to the computational time-step.

5.1. Self-Sustained Turbulence

Initially the magnetic and kinetic energies in the box increase, but the increase stops after around half an orbit, and then the magnetic and kinetic energies fall slowly to an equilibrium state during a transition time of around ten orbits. In the equilibrium state the turbulence is self-sustained, in the sense that energy is pumped from the gravitational field primarily into magnetic energy (via the magnetorotational instability). The Lorentz force transfers some of this magnetic energy into turbulent kinetic energy which again transfers energy back into the magnetic field in a dynamo process. Finally the energy is dissipated through resistivity and viscosity. The whole process is sketched in Brandenburg et al. (1995). Because we assume an isothermal equation of state, there is no heating of the gas due to dissipative processes.

The time evolution of kinetic energy components, magnetic energy components, and Reynolds and Maxwell stresses is shown in Fig. 1 for a time span of 100 orbits. All turbulence parameters are approximately constant in time, within a certain fluctuation interval, and show no sign of decaying after the steady state has set in after around ten orbits. Most of the kinetic energy (top panels) is present in the horizontal components of the velocity field, which is always measured relative to the Keplerian flow, whereas the vertical component contains a factor of two lower kinetic energy (this anisotropic trend is normal to MRI simulations, see e.g. Hawley et al. 1995). For the magnetic energy (middle panels), almost the entire energy is kept in the toroidal component of the magnetic field. The ratio between kinetic and magnetic energies stays approximately constant in time with the magnetic energy being a factor of around two higher than the kinetic energy. The Reynolds and Maxwell stresses (shown in the two bottom panels) can be converted into a turbulent viscosity and normalized to a turbulent α -value of Shakura & Sunyaev (1973). These values are shown for the different runs in the second and third columns of Table 2. The magnetic α -value is around a factor of four times the non-magnetic, so most angular momentum transport happens because of

magnetic fields. In the shearing sheet approximation the Keplerian background velocity is linear in space, so there is no pile-up of angular momentum anywhere in the box.

The magnetorotational instability injects energy at the largest scales of the box. The smaller scales are then set in motion as the large scale motion cascades down to smaller and smaller scales. Under the assumption that there is no pile-up of kinetic energy at any scales, the Fourier spectrum should obey a Kolmogorov-law $\tilde{u}(k) \sim k^{-1/3}$. The Fourier spectra of all velocity components for 64^3 and 128^3 runs are shown in Figs. 2 and 3. For reference a $k^{-1/3}$ line is shown. The spectra are averages taken from 10 to 100 orbits. At large scales, the power spectra approximately obey a Kolmogorov law, but at smaller scales, where dissipation becomes important, the slope becomes steeper. There is some excess power at the very smallest scales, especially for the 64^3 run. This is due to unstable modes at the smallest scales of the box. Curiously the excess power is only present in the radial and vertical directions and not in the toroidal direction, but this may be an effect of the shearing out of all variables along y . The power in the small scale modes is still negligible compared to the large scales, so the rise in power does not influence the diffusion of the dust. These rises in power are typical for simulations with a low diffusivity, see e.g. Haugen et al. (2004). According to mixing length theory, the contribution from the different length scales to the total turbulent diffusion coefficient scales as $D_k \sim \tilde{u}_k/k \sim k^{-4/3}$, so the largest scales of the box are expected to give the dominating contribution to the total turbulent diffusion coefficient.

One also sees from Figs. 2 and 3 that in both cases the vertical velocity amplitude on the large scales is smaller than the radial and toroidal velocity amplitude at large scales. This gives already a hint that vertical turbulent diffusion might be weaker than radial turbulent diffusion.

6. EVOLUTION OF DUST

The dust is initially at rest and has a constant number density $n(x, y, z) = n_0$. It is then set free to evolve under the influence of friction with the gas and the imposed gravity field. The dust begins to concentrate near the center of gravity (horizontal mid-plane, with $z = 0$, for vertical gravity, vertical mid-plane, with $x = 0$, for radial gravity), but eventually an equilibrium configuration is reached where the turbulent diffusion prevents further concentration. This situation is shown in Fig. 4 for a 128^3 run with $\Omega_0\tau_f = 2 \times 10^{-7}$ and vertical gravity. The run is labeled 128a_z in Table 1, and the friction time corresponds to tiny dust grains or molecules with radii of 0.2 micrometers in a typical solar nebula. The plot shows dust density contours at the sides of the simulation box. The turbulent motion

is clearly visible, and the resulting turbulent diffusion is the only reason why there is no further settling of the dust layer towards the mid-plane. The amplitude of the concentration around the mid-plane is maintained approximately constant for the entire duration of the simulation (one hundred orbits).

6.1. Diffusion Timescale

Before proceeding with measuring diffusion coefficients, we will first make an estimate of the time it takes to get from a constant dust density to the equilibrium where sedimentation is balanced by turbulent diffusion. We consider the case of vertical gravity. The logarithmic dust density must rise from an initial value $\ln n_0$ to the equilibrium value given by equation (21). When the amplitude of the equilibrium cosine function is small, $A_{\ln n} \ll 1$, then we can assume that $n_1 \approx n_0$. The increase in logarithmic dust density is then simply

$$\Delta \ln n = \frac{\tau_{\text{f}} g_0}{k_z D_z^{(t)}} \cos(k_z z). \quad (27)$$

This increase is caused by the vertical sedimentation. In the short friction time approximation the dust velocity can be written as $w_z = -\tau_{\text{f}} g_0 \sin(k_z z)$. The change in logarithmic dust density due to vertical settling can be approximated with the expression

$$\frac{\partial \ln n}{\partial t} = -\frac{\partial w_z}{\partial z} = k_z \tau_{\text{f}} g_0 \cos(k_z z). \quad (28)$$

Here we have ignored the advection of mass for simplicity. The diffusion timescale t_{D} can now be estimated by dividing equation (27) with equation (28). This yields

$$t_{\text{D}} = \frac{1}{k_z^2 D_z^{(t)}}. \quad (29)$$

Rewriting the diffusion coefficient in dimensionless units as $D_z^{(t)} = \delta_z^{(t)} c_s^2 \Omega_0^{-1}$, the diffusion timescale can be written as $\Omega_0 t_{\text{D}} = [(c_s \Omega_0^{-1} k_z)^2 \delta_z^{(t)}]^{-1}$. With $\Omega_0 = 0.2$, $k_z = 1$ and $\delta_z^{(t)} = 0.002$, the diffusion timescale is around three orbits. The diffusion timescale for radial diffusion is completely equivalent to equation (29).

For a linear gravity field, Dullemond & Dominik (2004) derive a diffusion timescale similar to equation (29). On the other hand, Dubrulle et al. (1995) state a diffusion timescale of $1/(\Omega_0^2 \tau_{\text{f}})$. This expression is actually a gravitational settling timescale that determines the amount of time it takes to increase the dust density in the mid-plane significantly due to gravity. Since the diffusion equilibrium sets in at very modest mid-plane overdensities for small dust grains, the timescale for such grains to reach diffusion equilibrium is much shorter than the gravitational settling timescale.

In Fig. 5 we plot the evolution of the logarithmic dust density averaged over the x - and y -directions for the run 64a $_z$. Starting at a time of zero orbits, curves are shown at two orbits time separation up to a time of ten orbits. The timescale to reach diffusion equilibrium is evidently around a few orbits (the saturated state is shown in Fig. 6). This is in good agreement with the analytical estimates given above.

6.2. Measured Turbulent Diffusion Coefficients

We now turn to measuring the turbulent diffusion coefficient from the equilibrium configuration that is illustrated in Fig. 4. According to equations (21) and (26), the equilibrium logarithmic dust density should be a cosine function if diffusion is the proper description of the turbulent transport. As an example of how the vertical diffusion coefficient is measured, we show in Fig. 6 the logarithmic dust density averaged over the radial and toroidal directions for the run 64a $_z$ at a time of $t = 38$ orbits. Also shown is the minimum χ^2 cosine fit (dotted line). The fit is excellent, and this shows that here the turbulent transport of the dust grains is well-described as diffusion. In Fig. 7 we plot, for the same run, the full time evolution of the amplitude of the best-fit cosine function and the quality of the fit, Q . The fit quality is defined as

$$Q \equiv \frac{\sum_i [\langle \ln n \rangle_{xy}(z_i) - (\ln n)_{\text{fit}}(z_i)]^2}{\sum_i [\langle \ln n \rangle_{xy}(z_i)]^2}. \quad (30)$$

Here the sum is taken over the entire vertical direction and $\langle \dots \rangle_{xy}$ is used to denote the average taken over the x - and y -directions. In Fig. 7 we also plot the turbulent diffusion coefficient derived from the amplitude using equation (21). Both the amplitude and the turbulent diffusion coefficient stay approximately constant in time. The fit quality fluctuates by more than an order of magnitude, but is generally very good (Q is less than 0.02 at all times). A similar behavior is found for all runs with short friction times, both for vertical and for radial gravity.

We have also run simulations without the short friction time approximation. Here the friction time must be at least a few times longer than the computational time-step of the gas in order to resolve the frictional acceleration in our explicit numerical scheme, but shorter than an orbital period for the fluid approach to be valid. We shall refer to such values of the friction time as intermediate friction times. Simulations with a freely evolving dust velocity serve both the purpose of showing in how far the short friction time approximation is valid, and also how the turbulent diffusion coefficient behaves when the friction time becomes larger and acceleration effects come into play. Remember that the short friction time approximation assumes that the dust grains can always reach an equilibrium velocity in one computational time-step. Hence effects such as vortex trapping in turbulent eddies

are not possible in the short friction time approximation. The time evolution of cosine amplitude, fit quality and turbulent diffusion coefficient for the intermediate friction time run 64c_x (with radial gravity and a friction time of $\Omega_0\tau_f = 0.02$ corresponding to dust grains with radii of a few centimeters) is shown in Fig. 8. Here the amplitude changes a lot with time, and the fit quality Q rises above 0.1 on several occasions. Apparently diffusion is not at all times a good description of the turbulent transport in this run, even though the grains are still relatively well-coupled to the gas. Nevertheless, the time averaged diffusion coefficient in Fig. 7 and Fig. 8 is approximately the same as for the small grains.

The measured turbulent diffusion coefficients in the vertical and radial directions are shown in Table 2. In Fig. 9 we plot the diffusion coefficients together with the α -value based on the Reynolds stress, α_t , and the α -value based on the Maxwell stress, $\alpha_t^{(\text{mag})}$. We include $1\text{-}\sigma$ fluctuation intervals on all measurements. The radial diffusion is seen to be much stronger (around 70%) than the vertical diffusion. This is also to be expected from Fig. 1, since the root-mean-square of the vertical velocity component is smaller than for the horizontal components, so the velocity fluctuations in the radial direction are stronger than in the vertical direction.

From the length of the fluctuation bars in Fig. 9, it is clear that the fluctuations in the turbulent diffusion coefficient are very small for the short friction time limit. Combined with the fact that the quality of the cosine fit is excellent, this means that the turbulent transport in that case is well-described as diffusion. For intermediate friction times, with a freely evolving dust velocity, the fluctuation in the turbulent diffusion coefficient becomes larger, especially in the radial direction. The average values of the diffusion coefficients nevertheless stay approximately constant both for short and intermediate friction times. This gives confidence in that the short friction time approximation is indeed valid for very small dust grains.

6.2.1. Diffusion Prandtl Number

It is of great interest to compare the measured diffusion coefficients with the turbulent viscosity, since a popular parametrization of turbulent diffusion is to set the diffusion coefficient equal to the turbulent viscosity coefficient. It is seen from Table 2 that the vertical diffusion coefficient is generally around a factor of three to four times the non-magnetic α -value, but the value is comparable to the magnetic α -value. The radial diffusion coefficient is slightly higher than the total turbulent α -value.

We quantify the difference between the measured turbulent diffusion coefficients and the

turbulent viscosity through the diffusion Prandtl number Pd . This is defined as the ratio between the turbulent viscosity and the turbulent diffusion coefficient as

$$\text{Pd} = \frac{\nu_t}{D_t}. \quad (31)$$

For anisotropic turbulence, the Prandtl number depends on the direction. Unfortunately there is no way to estimate the turbulent viscosity in the vertical direction, as there is no background shear and thus no flux of angular momentum vertically, so we shall use the value for the radial turbulent viscosity even for the vertical Prandtl number.

The measured Prandtl numbers are shown in the last two columns of Table 2. The vertical diffusion Prandtl number is found to be above unity in the range $\text{Pd}_z = 1.27 \dots 1.60$, while the radial diffusion Prandtl number is below unity in the range $\text{Pd}_x = 0.79 \dots 0.90$ and falling with increasing resolution. This is quite surprising as Prandtl numbers smaller than one could not be expected from standard diffusion theory. It is not possible to say whether the vertical Prandtl number would be similarly low if we had scaled with the proper vertical turbulent viscosity, because this quantity is, as mentioned above, not known.

6.2.2. Dependence on Particle Size

Much analytical work has been devoted to parametrizing the dependence of the diffusion coefficient on dust particle radius (Safronov 1969; Völk et al. 1980; Cuzzi et al. 1993; Dubrulle et al. 1995; Schräpler & Henning 2004; Reeks 2005). According to Schräpler & Henning (2004), ignoring the effect of the mean motion of the dust grains, the diffusion coefficient can be written as

$$D_t = \frac{D_0}{1 + \text{St}}. \quad (32)$$

Here St is the Stokes number, and the factor $1/(1 + \text{St})$ determines the variation of diffusion coefficient with particle radius. The Stokes number is defined as the ratio of the friction time to the turn-over time τ_c of the largest eddies. Assuming that the rotation speed of the largest eddies as $v_e = \alpha_t^q c_s$ and choosing $q = 0.5$, one can (following Schräpler & Henning 2004) derive the expression

$$D_t = \frac{D_0}{1 + 4^{-1} \pi \Omega_0 \tau_f}. \quad (33)$$

Thus for the largest grains considered in this work, with $\Omega_0 \tau_f = 0.02$, the expected change in diffusion coefficient due to particle size is around 1.5%. This is well below the fluctuation intervals in the measurements. Our results indeed confirm that there is no apparent size-dependence on the measured diffusion coefficient for our chosen grain size range. This also confirms the interpretation that the variation in the observed disc thickness at various

wavelengths is due to differential settling between particles of different sizes (e.g. Dullemond & Dominik 2004) and not due to a variation in the diffusion coefficient with particle size.

6.3. Local Dust Density Enhancement

To explore why the diffusion coefficient fluctuates so much in the intermediate friction time runs, we plot in Fig. 10 the dust-to-gas ratio probability function for an intermediate friction time run with $\Omega_0\tau_f = 0.02$ (full line) and a short friction time run with $\Omega_0\tau_f = 2 \times 10^{-7}$ (dotted line) for a resolution of 64^3 and no gravity. These two gravity-free runs are named 64c_ng and 64a_ng, respectively. The probability of a grid point having a dust-to-gas ratio between ϵ_d and $\epsilon_d + \Delta\epsilon_d$ is

$$p(\epsilon_d) = \frac{\Delta f(\epsilon_d)}{\Delta\epsilon_d}, \quad (34)$$

where $\Delta f(\epsilon_d)$ is the fraction of all grid points in the simulation box having a dust-to-gas ratio between ϵ_d and $\epsilon_d + \Delta\epsilon_d$. We average over 10 orbits taken equidistantly between orbits 10 and 100. According to Fig. 10 the probability of finding grid points with very high or very low dust-to-gas ratios is much higher in the intermediate friction time run than in the short friction time run. The dust-to-gas ratio in the short friction time run is extremely peaked around $\epsilon_d = \epsilon_0$, thus only the bottom part of the curve could be shown in Fig. 10. The full curve is shown in Fig. 11.

There are two potential sources for the high dust-to-gas ratio contrast that is seen in the intermediate friction time: trapping of dust grains in turbulent vortices or trapping in regions of high pressure by pressure gradient trapping, as mentioned in the introduction. The latter effect can work also in the short friction time approximation, the first can not. According to equation (11), the terminal velocity of small dust grains climbing up the local pressure gradient is (we ignore gas velocity and set external gravity to zero)

$$\mathbf{w} = \tau_f[\rho^{-1}(\nabla P - \mathbf{J} \times \mathbf{B})]. \quad (35)$$

The evolution of the dust number density of a fluid element is controlled by the continuity equation

$$\frac{D \ln n}{Dt} = -\nabla \cdot \mathbf{w}, \quad (36)$$

where $D/Dt \equiv \partial/\partial t + (\mathbf{w} \cdot \nabla)$ is the advective derivative of the flow. Combining equation (36) with equation (35) shows that dust should concentrate in regions where $\nabla \cdot [\rho^{-1}(\nabla P - \mathbf{J} \times \mathbf{B})] \equiv \nabla \cdot \mathbf{F} < 0$ and be removed from regions where the divergence is negative. We examine whether this is the case in the two bottom panels of Fig. 12. Here the average dust-to-gas ratio (including 1- σ fluctuation intervals) is shown for bins in $\nabla \cdot \mathbf{F}$. The left

panel is for the short friction time run 64a_ng while the right panel is for the intermediate friction time run 64c_ng. For the intermediate friction time run, there is evidently some correlation between a positive divergence and a low dust-to-gas ratio and vice versa, but the correlation is not very strong.

Vortex trapping is another potential source of the dust-to-gas ratio contrast (Barge & Sommeria 1995). It can be very powerful when $\Omega_0\tau_f$ is close to unity. The delayed acceleration of a dust grain entering a turbulent gas eddy causes the Coriolis force to dominate completely over the centrifugal force of the eddy. The effect of vortex trapping can be seen from the vorticity $\boldsymbol{\omega} \equiv \nabla \times \mathbf{u}$ of the flow. Cyclonic vortices (with positive ω_z) have an outwards directed Coriolis force relative to the center of motion and can expel dust grains. Anticyclonic vortices (with negative ω_z) have a Coriolis force that points inwards. Such vortices can trap dust grains. As an illustration of the trapping of dust grains in turbulent features we show in Fig. 13 contour plots of ω_z and ϵ_d in an arbitrarily chosen x - y -plane. The vorticity contours show patches of positive and negative vorticity. The correlation between negative vorticity and high dust-to-gas ratio (and vice versa) is clearly seen in many places. However, it is not a perfect 1:1 fit, as can also be expected in a dynamical system that is changing all the time. All concentrations are only surviving as long as a vortex exists. Turbulent eddies have a lifetime comparable to the shear time of the system, i.e. the orbital period.

It is easier to see the correlation between vertical vorticity and dust-to-gas ratio in Fig. 12. Here the three top rows show the correlation between dust-to-gas ratio and the three directional components of the vorticity. There is a strong correlation with vertical vorticity component ω_z for the intermediate friction time run. This is exactly as expected in case vortex trapping and expelling is the source of the number density contrast. A vertical vorticity can however also be caused by a non-rotating flow, e.g. if the gas-flow is hyper-Keplerian with a shear velocity that is linear with the radial coordinate $u_y \propto x$. Such a profile can be caused by a radial bump in the gas density. Here dust-trapping would be due to pressure gradient trapping and not due to vortex trapping.

A better test of vortex trapping than vertical vorticity can be devised by taking a closer look at the trapping mechanism (see e.g. Johansen et al. 2004). An anticyclonic vortex is in equilibrium because there is a resulting force on the gas particles pointing towards the center of rotation. This resulting force is a vector sum of the Coriolis force, the pressure gradient force and the Lorentz force, and it works as a centripetal force that supplies just the right amount of force necessary to orbit the center of rotation. In the fluid equations, the resulting centripetal force is balanced by the additional advection term that keeps the velocity field unchanged, even though the fluid elements themselves experience an acceleration towards

the center of rotation. Thus for anticyclonic vortices, the advection vector $-(\mathbf{u} \cdot \nabla)\mathbf{u}$ points away from the center of rotation, while the Coriolis force $\mathbf{f}(\mathbf{u})$ points towards the center of rotation, which is exactly in the opposite direction. The occurrence of the Coriolis force pointing in the opposite direction of the advection vector is a sufficient condition for having an anticyclonic vortex and thus vortex trapping. For a cyclonic vortex both the Coriolis force and the advection vector point away from the center of rotation. Defining the vortex parameter $\Psi \equiv [-(\mathbf{u} \cdot \nabla)\mathbf{u}] \cdot \mathbf{f}(\mathbf{u})$, we can now recognize cyclones by a positive value of Ψ and anticyclones by a negative value of Ψ . If dust grains are affected by vortex trapping, then there should be an anticorrelation between Ψ and the dust-to-gas ratio at the locations of cyclones and anticyclones. We examine this in Fig. 14. It is seen that the anticorrelation between Ψ and dust-to-gas ratio is significant. This allows us to conclude that the large fluctuations in dust-to-gas ratio for the intermediate friction time runs is caused by trapping in turbulent eddies.

Curiously there is also a significant correlation between any non-zero toroidal vorticity component ω_y and a low dust-to-gas ratio for the intermediate friction time run in Fig. 12. This may be related to dust grains being expelled from eddies with a rotation axis parallel to the mid-plane (in the absence of gravity; when vertical gravity is included, particles can become suspended in such eddies, see Klahr & Henning 1997; Pasquero et al. 2003). However, there is no similar correlation with the radial component of vorticity ω_x , probably because the shear wipes out any depletions/concentrations on a very short timescale.

A similar search for concentrations of dust grains in MRI turbulence was performed by Hodgson & Brandenburg (1998). They find that for a frozen gas velocity field, intermediate friction time dust grains do indeed concentrate in the turbulent gas structures, but they attribute this effect to dust grains concentrating where the gas velocity field is converging rather than to vortex trapping. For an evolving gas velocity field, they find no concentration of dust. It is not clear why our results differ from these results. However, Hodgson & Brandenburg (1998) focus on concentrations of dust particles in the vertical plane, while in the current work dust concentrations are most pronounced in rotating structures in the horizontal plane.

7. CONCLUSIONS

The transport properties of dust grains in a turbulent accretion disc is of interest for many aspects of protoplanetary disc modeling and planet formation scenarios. In this paper, we have measured the turbulent diffusion coefficient of dust grains embedded in ideal MHD magnetorotational turbulence directly from numerical simulations. The choice of magne-

torotational turbulence was made because there is a growing realization that the magnetorotational instability can work at least in some parts of protoplanetary discs, even where the ionization fraction may be surprisingly low. It is also routinely produced in shearing box simulations, so it is a very accessible form of turbulence. Thus, by the use of MRI, we have a natural source of turbulence, whereas the current only other alternative for similar studies would be the use of driven turbulence in a box. The use of the ideal MHD equations can only be justified as a first approach to calculate the turbulent transport properties of dust grains. Further studies of non-ideal MHD should be made to clarify the transport properties of grains deeply embedded in the disc where the ionization fraction is low and where one is confronted with a “dead zone” around the mid-plane of the disc.

As a numerical solver we have used the Pencil Code. This finite difference code solves the non-conservative form of the dynamical equations. It is special compared to other codes in that it uses sixth order derivatives in space. The numerical scheme of the Pencil Code was stabilized using hyperdiffusivity terms in all the dynamical equations. The effect of hyperdiffusivity is to affect the large scale motion as little as possible, while at the same time quenching unstable modes at the smallest scales of the box. By varying the size of the artificial diffusion coefficient, we have found the direct influence of artificial diffusion on the measured turbulent diffusion coefficient to be negligible, most likely due to the fact that mass diffusion is primarily contributed by the fast and far moving large scales of the turbulence, and these are as mentioned affected only very little by hyperdiffusivity. From this perspective, hyperdiffusivity seems to be a tool that is well suited for measurements of turbulent transport properties.

Since we have only considered dust grains of sizes much less than one meter, the dust grains could be treated as a fluid interacting with the gas through a drag force. For the tiniest dust grains, where the friction time is much shorter than the computational time-step, we have used an algebraic equation to obtain the dust velocity at each time-step. This short friction time approximation incorporates the tendency of dust grains to move up the local pressure gradient of the gas, an effect which we have referred to as pressure gradient trapping. It can explain such phenomena as the settling of dust grains towards the mid-plane of a stratified disc and the radial drift of dust grains in discs with a radial pressure gradient. In the current work, we have also included the effects of magnetic pressure and tension in the short friction time approximation. For intermediate friction time dust grains, where the friction time is within a few orders of magnitude of the orbital period, we have integrated the dust equation of motion together with the other dynamical equations. Here acceleration effects are allowed, in the sense that dust grains are no longer assumed to instantaneously reach a terminal velocity where the drag force is balanced by the other forces affecting the dust. The fact that the time average of the measured diffusion coefficient was approximately

the same for tiny dust grains, using the short friction time approximation, and intermediate size dust grains, with a free evolution of the dust velocity, gives some credit to the validity of the short friction time approximation.

We have chosen to measure the turbulent diffusion coefficient by forcing the dust grains to settle towards a mid-plane by an external force field. This settling was eventually balanced by turbulent diffusion away from the mid-plane. To deduce the value of the turbulent diffusion coefficient, the equilibrium dust density could then be compared with an analytical solution for a parametrized diffusion coefficient. The method works not only for the vertical direction, but also for the radial direction, so that we have been able to measure both the vertical and the radial turbulent diffusion coefficients.

For the short friction time runs, the equilibrium dust number density was excellently fitted with the expected analytical solution. That means that the turbulent transport of small dust grains is well-described as diffusion. For intermediate friction times, the equilibrium dust number density was much more erratic, especially in the radial direction, and did not always give a good fit. We also found that the dust-to-gas ratio probability distribution was much wider than in the short friction time runs. To explore the reason for the large spread in dust-to-gas ratio, we have examined correlations between different parameters of the gas and the dust-to-gas ratio. A strong correlation between vertical vorticity component and dust-to-gas ratio was found. Based on this and an equally strong correlation between the sign of the vortex parameter and the dust-to-gas ratio, we conclude that the spread in dust-to-gas ratio, and thus the fluctuations in the diffusion coefficient, is due to vortex trapping in turbulent eddies (Barge & Sommeria 1995). Some weaker indications that pressure gradient trapping is taking place were also found, but similar to the results of Johansen et al. (2004), the over all dominant trapping mechanism is found to be vortex trapping. The dust-trapping that is seen in the current work happens for relatively well-coupled particles with a friction time on the order of a few percent times the shear time Ω_0^{-1} . One can speculate that for larger particles, dust-trapping mechanisms will be so efficient that the diffusion picture of turbulent transport will no longer be valid, but further investigations into the transport of larger particles will have to examine this. Such an investigation would have to incorporate dust grains as particles moving on top of the gas fluid, since the fluid description of dust grains is no longer valid when the mean free path becomes larger than the scale height of the disc.

In the vertical direction the turbulent diffusion coefficient was measured to be smaller than the total turbulent viscosity and have a diffusion Prandtl number of approximately $\text{Pd}_z = 1.5$. The diffusion coefficient is still considerably larger than the non-magnetic turbulent viscosity alone. The measured radial turbulent diffusion coefficient turned out to be

almost twice as large as the vertical diffusion coefficient. It is systematically larger than the total turbulent viscosity, i.e. the sum of the non-magnetic and the magnetic turbulent viscosity, with a diffusion Prandtl number of around $\text{Pd}_x = 0.85$. The value of the radial diffusion Prandtl number was found to be falling with increasing resolution. Future simulations should try to find convergence for the diffusion Prandtl numbers, but this is beyond the scope of the present work.

The anisotropy between the vertical and the radial directions should be taken into account for studies of planetesimal formation which invoke a gravitational instability in the dust sublayer. Here the onset of a gravitational instability in the vertically settled dust layer depends strongly on the effect of vertical diffusion. The amount of anisotropy can be expected to increase if the effect of vertical gravity and stratification is included (S. Fromang, personal communication), since then the buoyancy of the gas would decrease the vertical velocity fluctuations.

We want to stress that even though we find a radial diffusion Prandtl number of less than unity, the disc can still be assumed to radially transport dust grains and angular momentum about equally well. This is important for the modeling of radial mixing of dust grains and chemical species, a task which is becoming ever more relevant as more observations of the radial distribution of dust grains and molecules in protoplanetary discs become available. The result is in agreement with Yousef et al. (2003), who find for simulations of forced MHD turbulence a turbulent magnetic Prandtl number of unity. For dust grains, the equality between the radial turbulent diffusion coefficient and the turbulent viscosity is surprising, when considering that most of the angular momentum is transported by magnetic Maxwell stresses, while the dust grains have no coupling with magnetic fields at all. Following the argument of Tennekes & Lumley (1972), both angular momentum transport by Reynolds stresses and radial diffusion depend on the radial velocity fluctuations, so one would expect the non-magnetic α -value and the diffusion coefficient to be similar. The actual cause of the measured mismatch between turbulent diffusion and non-magnetic turbulent viscosity would seem to need more discussion in the future.

AJ wishes to acknowledge the kind hospitality of Anja Andersen and Axel Brandenburg at NORDITA in Copenhagen during part of this work. We wish to thank Cornelis Dullemond for many inspirational discussions on the observational consequences of dust diffusion. We are also grateful to Coryn Bailer-Jones for his many suggestions of language improvements to the original manuscript. Computer simulations were performed at the Danish Center for Scientific Computing in Odense. Our work is supported in part by the European Community's Human Potential Programme under contract HPRN-CT-2002-00308, PLANETS.

A. HYPERDIFFUSIVITY

In this appendix we discuss the use of hyperdiffusivity and present the hyperversions of viscosity, mass diffusion and resistivity that we are applying in this work.

Because the Pencil Code is a finite-difference code, artificial diffusivity terms are needed in all dynamical equations to stabilize the numerical scheme. For this purpose, we use sixth order hyperdiffusivity terms which affect mainly high wave numbers, the smallest scales in the simulation, and preserve the energy at low wave numbers. Hyperviscosity and magnetic hyperdiffusivity have been used extensively to study the properties of forced magnetohydrodynamical turbulence (e.g. Brandenburg & Sarson 2002, and references therein). The prospect is to affect large scales as little as possible by dissipation, thus widening the inertial range beyond what can be achieved with a regular viscosity operator.

Possible side effects of using hyperviscosity and magnetic hyperdiffusivity is to increase the bottleneck effect (a physical effect in turbulence where energy piles up around the dissipative scale, see e.g. Müller & Biskamp 2000) and to cause the dynamo-generated magnetic field in helical flows to saturate at a higher level than what is seen when using a regular viscosity operator (Brandenburg & Sarson 2002). Nevertheless, for forced non-magnetic turbulence Haugen & Brandenburg (2004) show that the shape of the inertial range for runs with hyperviscosity is very similar to the shape for higher resolution runs without hyperviscosity.

For the current work we define a momentum-conserving hyperviscosity function \mathbf{f}_ν as

$$\mathbf{f}_\nu(\mathbf{u}, \rho) = (-1)^{m-1} \rho^{-1} \nabla \cdot (\nu_m \rho \mathbf{S}^{(2m-1)}). \quad (\text{A1})$$

Here $\mathbf{S}^{(l)}$ is a simplified l th order rate-of-strain tensor defined as

$$S_{ij}^{(l)} = \frac{\partial^l u_i}{\partial x_j^l}. \quad (\text{A2})$$

For computational simplicity we consider the dynamical viscosity $\mu_m \equiv \nu_m \rho$ to be constant. Then the hyperviscosity function takes the appearance

$$\mathbf{f}_\nu(\mathbf{u}, \rho) = (-1)^{m-1} \frac{\mu_m}{\rho} \nabla^{2m} \mathbf{u}, \quad (\text{A3})$$

where $\nabla^{2m} \equiv \nabla_x^{2m} + \nabla_y^{2m} + \nabla_z^{2m}$ is a high order differential operator that reduces to a Laplacian for $m = 1$. For the purpose of stabilizing the numerical scheme we adopt a sixth order hyperviscosity by setting $m = 3$ in equation (A3). The hyperviscosity function \mathbf{f}_ν then appears as

$$\mathbf{f}_\nu(\mathbf{u}, \rho) = \frac{\mu_3}{\rho} \nabla^6 \mathbf{u}. \quad (\text{A4})$$

For the artificial mass diffusion term we define the hyperdiffusion function f_D as

$$f_D(\rho) = (-1)^{m-1} D_m \nabla^{2m} \rho, \quad (\text{A5})$$

where D_m is a constant diffusion coefficient. Using f_D as a diffusion term in the continuity equation conserves mass density. Again we adopt a hyperdiffusivity version with $m = 3$, leading to the expression

$$f_D(\rho) = D_3 \nabla^6 \rho. \quad (\text{A6})$$

The hyperresistivity function \mathbf{f}_η is defined as

$$\mathbf{f}_\eta(\mathbf{A}) = (-1)^{m-1} \eta_m \nabla^{2m} \mathbf{A}, \quad (\text{A7})$$

where η_m is the magnetic diffusivity. As for viscosity and diffusion we use a hyperresistivity scheme with $m = 3$ in equation (A7). Then the resistivity function \mathbf{f}_η comes out as

$$\mathbf{f}_\eta(\mathbf{A}) = \eta_3 \nabla^6 \mathbf{A}. \quad (\text{A8})$$

Using this function as a resistivity term in the induction equation conserves all components of the magnetic field \mathbf{B} .

B. RADIAL DIFFUSION EQUILIBRIUM

In this appendix we derive the equilibrium dust density when the dust is exposed to a radial gravity. We define a sinusoidal gravity field similar to what was done in the z -direction as

$$g_x = -g_0 \sin(k_x x), \quad (\text{B1})$$

where $k_x = 2\pi/L_x$ is the radial wave number of the field. In the horizontal plane the Coriolis force connects the radial and toroidal motions, so that any velocity in one direction results in an acceleration in the other direction. If not for the damping effect of friction, dust grains starting with any non-zero velocity would be forced to move in epicyclic motion. Fortunately the drag force from the gas permits an equilibrium solution to the dust equation of motion equation (5). We solve for $\mathbf{u} = w_z = 0$, $w_x = w_x(x)$ and $w_y = w_y(x)$ and get the two component equations of the equation of motion

$$0 = -w_x \frac{\partial w_x}{\partial x} + 2\Omega_0 w_y - \frac{1}{\tau_f} w_x - g_0 \sin(k_x x), \quad (\text{B2})$$

$$0 = -w_x \frac{\partial w_y}{\partial x} - \frac{1}{2} \Omega_0 w_x - \frac{1}{\tau_f} w_y. \quad (\text{B3})$$

Again the advection is ignored. This leads to an algebraic linear system of equations in w_x and w_y ,

$$0 = 2\Omega_0 w_y - \frac{1}{\tau_f} w_x - g_0 \sin(k_x x), \quad (\text{B4})$$

$$0 = -\frac{1}{2}\Omega_0 w_x - \frac{1}{\tau_f} w_y, \quad (\text{B5})$$

that has the solution

$$\begin{cases} w_x &= -\frac{\tau_f g_0}{1+\Omega_0^2 \tau_f^2} \sin(k_x x) \approx -\tau_f g_0 \sin(k_x x) \\ w_y &= \frac{\Omega_0 \tau_f^2 g_0}{2(1+\Omega_0^2 \tau_f^2)} \sin(k_x x) \approx \frac{1}{2}\Omega_0 \tau_f^2 g_0 \sin(k_x x) \end{cases} . \quad (\text{B6})$$

Here the approximate expressions are valid to first order in $\Omega_0 \tau_f$. The ratio between toroidal and radial velocity is $|w_y/w_x| = \frac{1}{2}\Omega_0 \tau_f$, so the toroidally imposed velocity becomes unimportant with sufficiently short friction time. For this form of velocity field, the equilibrium continuity equation takes the form

$$0 = -\frac{\partial}{\partial x} \left[w_x(x) n(x, y) - D_x^{(t)} \frac{\partial n(x, y)}{\partial x} \right] - \frac{\partial}{\partial y} \left[\{w_y(x) + u_y^{(0)}(x)\} n(x, y) - D_y^{(t)} \frac{\partial n(x, y)}{\partial y} \right]. \quad (\text{B7})$$

By considering solutions to equation (B7) of the form $n(x, y) = n(x)$, the y -derivative term of equation (B7) vanishes entirely. Then the equilibrium solution to the continuity equation, when assuming that the total flux of number density radially through the box is zero, is simply

$$\ln n = \ln n_1 + \frac{\tau_f g_0}{k_x D_x^{(t)}} \cos(k_x x), \quad (\text{B8})$$

formally identical to the vertical case.

REFERENCES

- Arlt, R., & Rüdiger, G. 2001, *A&A*, 374, 1035
- Armitage, P. J. 1998, *ApJ*, 501, L189+
- Balbus, S. A., & Hawley, J. F. 1991, *ApJ*, 376, 214
- Balbus, S. A., & Hawley, J. F. 1998, *Reviews of Modern Physics*, 70, 1
- Barge, P., & Sommeria, J. 1995, *A&A*, 295, L1
- Blum, J., & Wurm, G. 2000, *Icarus*, 143, 138

- Bockelée-Morvan, D., Gautier, D., Hersant, F., Huré, J.-M., & Robert, F. 2002, *A&A*, 384, 1107
- van Boekel, R., Min, M., Leinert, C., Waters, L. B. F. M., Richichi, A., Chesneau, O., Dominik, C., Jaffe, W., Dutrey, A., Graser, U., Henning, T., de Jong, J., Köhler, R., de Koter, A., Lopez, B., Malbet, F., Morel, S., Paresce, F., Perrin, G., Preibisch, T., Przygodda, F., Schöller, M., & Wittkowski, M. 2004, *Nature*, 432, 479
- Boss, A. P. 2003, *ApJ*, 599, 577
- Brandenburg, A., Nordlund, Å., Stein, R.F., & Torkelsson, U. 1995, *ApJ*, 446, 741
- Brandenburg, A., & Sarson, G. R. 2002, *Physical Review Letters*, 88, 055003
- Brandenburg, A. 2003, in *Advances in nonlinear dynamos (The Fluid Mechanics of Astrophysics and Geophysics, Vol. 9)*, ed. A. Ferriz-Mas & M. Núñez (Taylor & Francis, London and New York), 269-344
- Chavanis, P. H. 2000, *A&A*, 356, 1089
- Cuzzi, J. N., Dobrovolskis, A. R., & Champney, J. M. 1993, *Icarus*, 106, 102
- Cuzzi, J. N., Hogan, R. C., Paque, J. M., & Dobrovolskis, A. R. 2001, *ApJ*, 546, 496
- Dubrulle, B., Morfill, G., & Sterzik, M. 1995, *Icarus*, 114, 237
- Dubrulle, B., Marié, L., Normand, C., Richard, D., Hersant, F., & Zahn, J.-P. 2005, *A&A*, 429, 1
- Dullemond, C. P. 2002, *A&A*, 395, 853
- Dullemond, C. P., & Dominik, C. 2004, *A&A*, 421, 1075
- Fleming, T., & Stone, J. M. 2003, *ApJ*, 585, 908
- Fromang, S., Terquem, C., & Balbus, S. A. 2002, *MNRAS*, 329, 18
- Goldreich, P. & Tremaine, S. 1978, *ApJ*, 222, 850
- Hanner, M. S. 1999, *Space Science Reviews*, 90, 99
- Haugen, N. E., Brandenburg, A., & Dobler, W. 2004, *Phys. Rev. E*, 70, 016308
- Haugen, N. E., & Brandenburg, A. 2004, *Phys. Rev. E*, 70, 026405

- Hawley, J. F., Gammie, C. F., & Balbus, S. A. 1995, *ApJ*, 440, 742
- Hodgson, L. S., & Brandenburg, A. 1998, *A&A*, 330, 1169
- Ilgner, M., Henning, T., Markwick, A. J., & Millar, T. J. 2004, *A&A*, 415, 643
- Johansen, A., Andersen, A. C., & Brandenburg, A. 2004, *A&A*, 417, 361
- Klahr, H. H., & Henning, T. 1997, *Icarus*, 128, 213
- Klahr, H. H., & Bodenheimer, P. 2003, *ApJ*, 582, 869
- Klahr, H. 2004, *ApJ*, 606, 1070
- Klahr, H. H., & Bodenheimer, P. 2005, submitted to *ApJ*
- Li, H., Finn, J. M., Lovelace, R. V. E., & Colgate, S. A. 2000, *ApJ*, 533, 1023
- Lin, D. N. C., & Papaloizou, J. 1980, *MNRAS*, 191, 37
- Müller, W., & Biskamp, D. 2000, *Physical Review Letters*, 84, 475
- Norton, O. R. 2002, *The Cambridge Encyclopedia of Meteorites* (Cambridge University Press, 2002)
- Pasquero, C., Provenzale, A., & Spiegel, E. A. 2003, *Physical Review Letters*, 91, 054502
- Reeks, M. W. 2005, *Journal of Fluid Mechanics*, 522, 263
- Ryu, D., & Goodman, J. 1992, *ApJ*, 388, 438
- Safronov, V. S. 1969, *Evoliutsiia doplanetnogo oblaka*. (English transl.: *Evolution of the Protoplanetary Cloud and Formation of Earth and the Planets*, NASA Tech. Transl. F-677, Jerusalem: Israel Sci. Transl. 1972)
- Schräpler, R. & Henning, T. 2004, *ApJ*
- Semenov, D., Wiebe, D., & Henning, T. 2004, *A&A*, 417, 93
- Shakura, N. I., & Sunyaev, R. A. 1973, *A&A*, 24, 337
- Shalybkov, D., & Rüdiger, G. 2005, *astro-ph/0501154*
- Tennekes, H., & Lumley, J. L. 1972, *First Course in Turbulence* (Cambridge: MIT Press, 1972)

Völk, H. J., Morfill, G. E., Roeser, S., & Jones, F. C. 1980, *A&A*, 85, 316

Weidenschilling, S. J. 1977, *MNRAS*, 180, 57

Yousef, T. A., Brandenburg, A., & Rüdiger, G. 2003, *A&A*, 411, 321

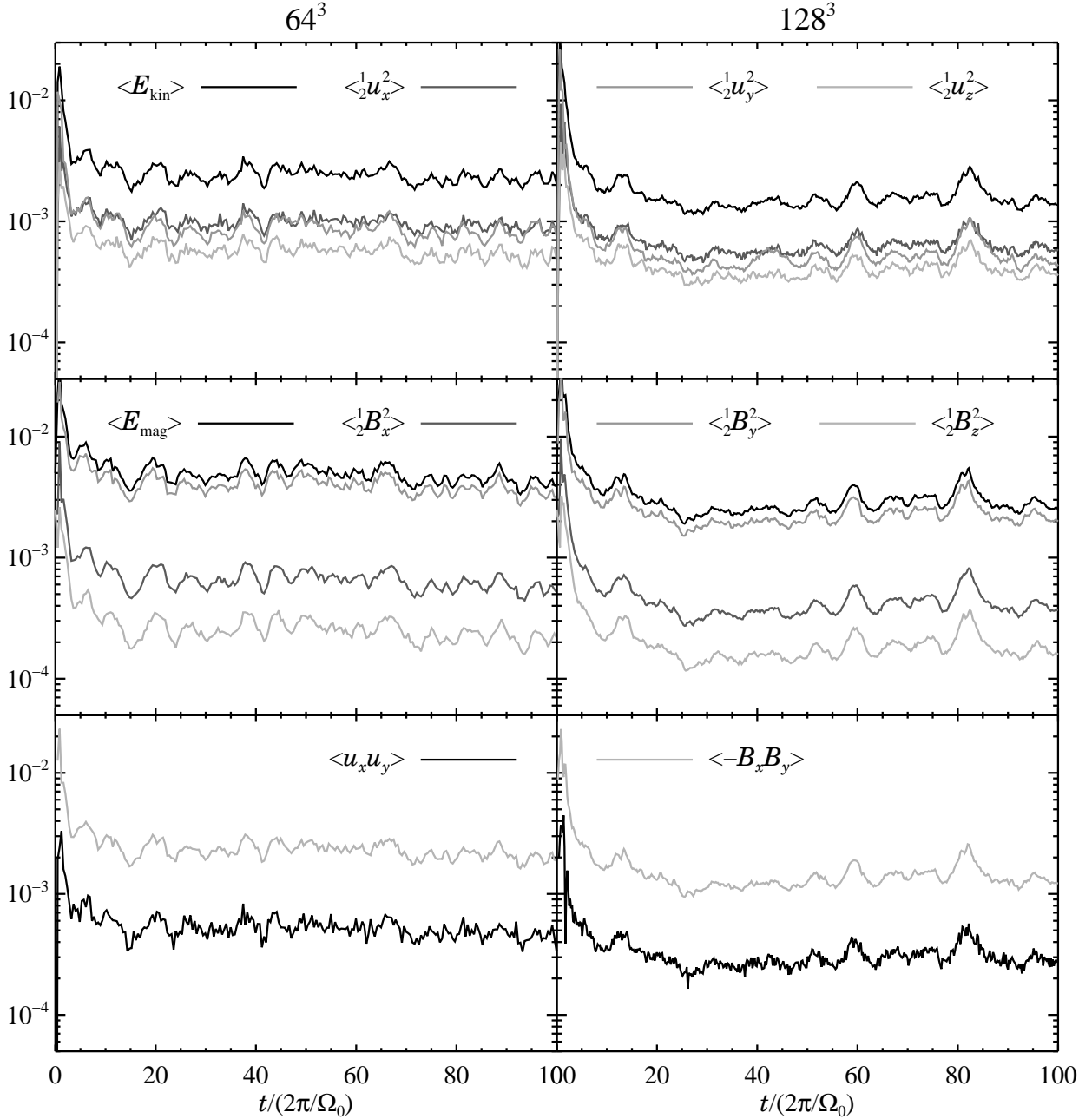


Fig. 1.— Evolution of various turbulence parameters for a 64^3 run (left panels) and a 128^3 run (right panels). The top panels show the evolution of total kinetic energy and its directional components. The radial and toroidal directions have comparable values of kinetic energy, whereas the vertical direction has around a factor of two less. The magnetic energy (middle panels) is completely dominated by the toroidal magnetic field. The uy component of the Reynolds and Maxwell stresses (lower panels) is effectively a measure of the turbulent viscosity. The magnetic stresses are around four times higher than the kinetic stresses.

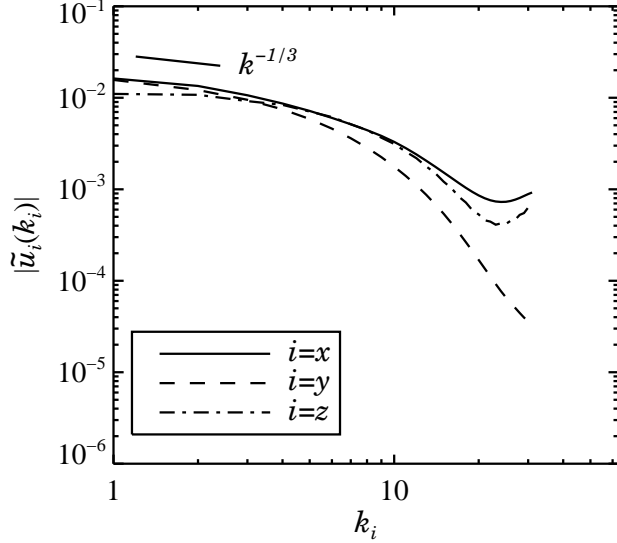


Fig. 2.— Fourier spectrum of the velocity components of the gas for a 64^3 resolution run, averaged from 10 to 100 orbits. A Kolmogorov $k^{-1/3}$ line is shown for reference. Both the radial and the toroidal components show a Kolmogorov-like behavior on large scales, whereas the vertical component is flatter. At small scales dissipation becomes important. The radial and vertical directions show a rise in power on the very smallest scales.

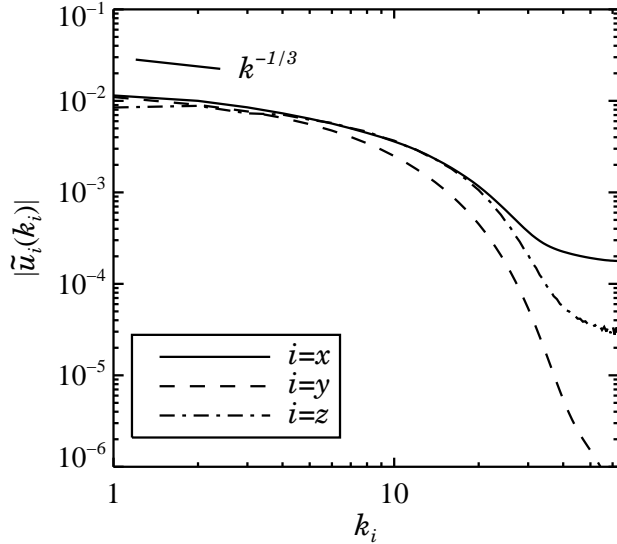


Fig. 3.— Same as Fig. 2, but for a 128^3 resolution run. The vertical velocity component still has a flatter slope in the inertial range than the two other components, but the surplus power at the very smallest scale is greatly diminished compared to the 64^3 run.

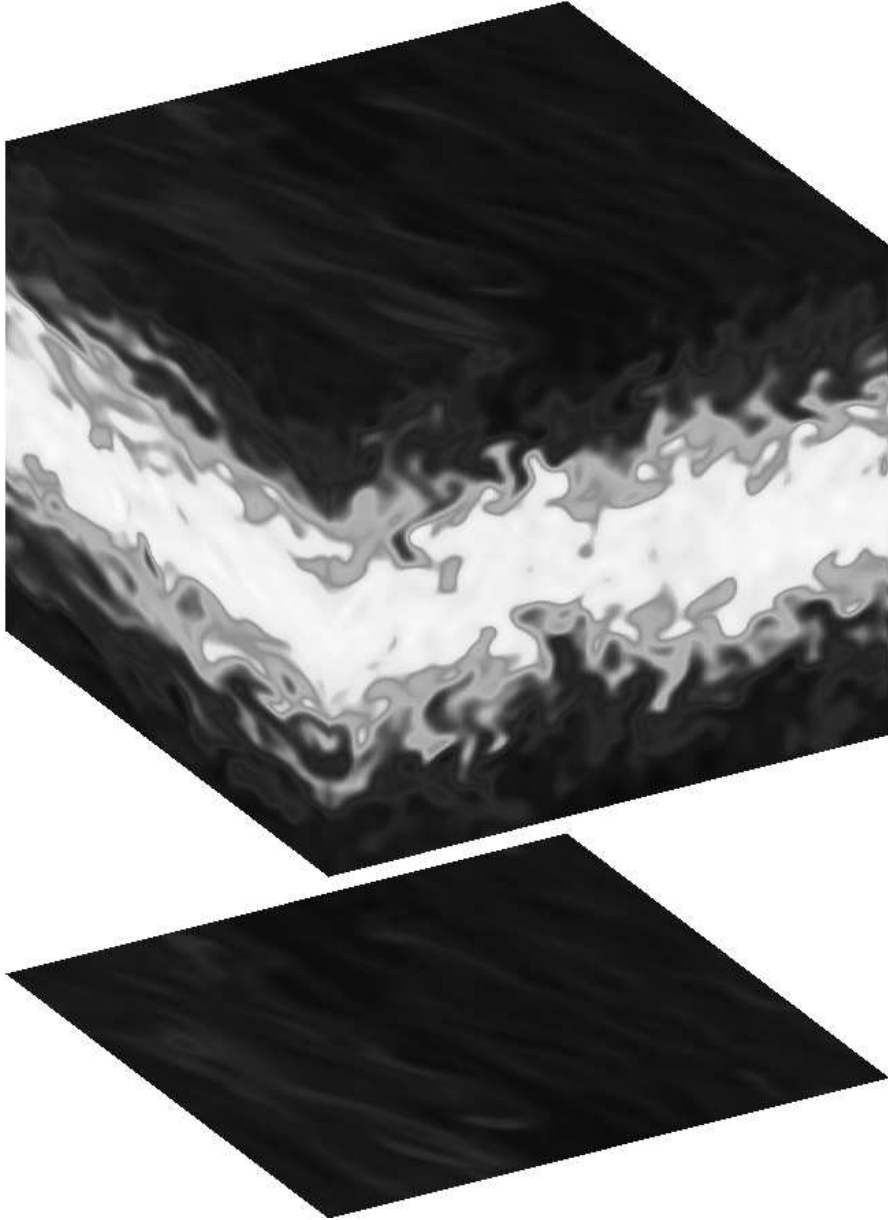


Fig. 4.— Dust density contours at the sides of the simulation box for the short friction time run 128a_z. The radial direction is towards the right while the shearing direction is towards left. The dust is concentrated around the mid-plane due to a vertical gravity acting only on the dust. Turbulent transport alone prevents the further vertical settling of the dust layer. This configuration is statistically unchanged for at least one hundred orbits.

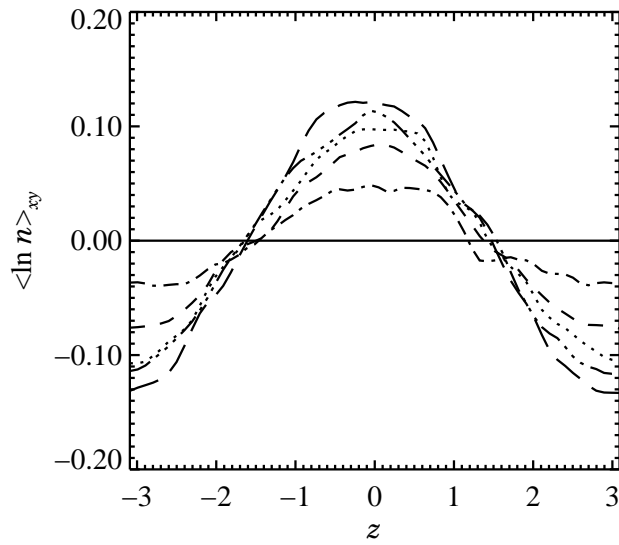


Fig. 5.— The logarithmic dust density of the run 64a_z, averaged over x and y , at different times. The curves are each separated by two orbits going from $t = 0$ (full line) to $t = 10$ orbits (long-dashed line). The approach to equilibrium happens on a timescale of a few orbits, in good agreement with the analytical estimate of the diffusion timescale that is presented in the text.

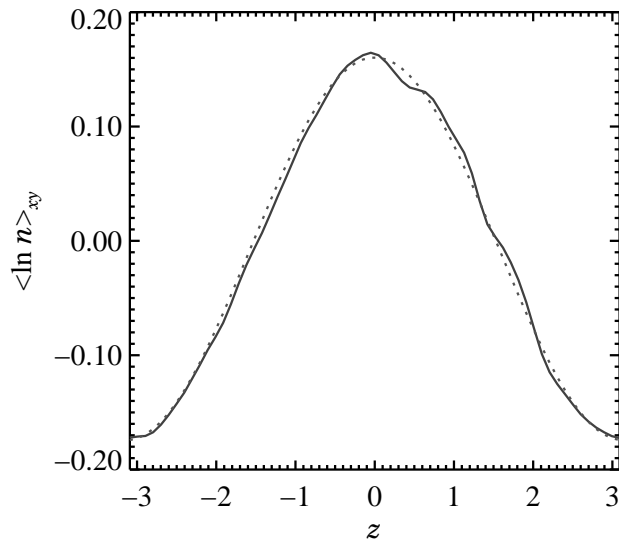


Fig. 6.— The logarithmic dust density averaged over x and y as function of vertical height z (full line) and a cosine fit (dotted line). The cosine fit is in excellent agreement with the data. This shows that the turbulent transport is indeed well described as diffusion. Shown here is for the short friction time run 64a $_z$ at a time of 26 orbits. The fit quality (defined in the text) is $Q \approx 0.005$.

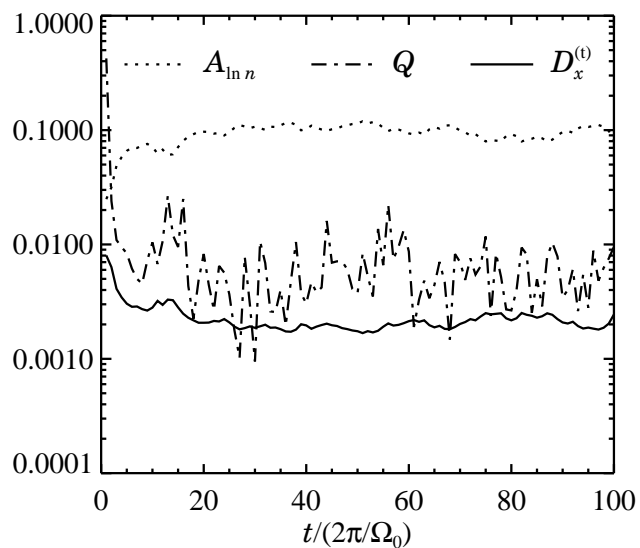


Fig. 7.— Time evolution of the fitted cosine amplitude (dotted line), the fit quality (dash-dotted line) and the derived radial turbulent diffusion coefficient (full line) for the short friction time run 64a_x with radial gravity. Both the fit amplitude, and hence the turbulent diffusion coefficient, are approximately constant in time, although small variations are seen. The fit quality is generally excellent, but it fluctuates with around an order of magnitude during the 100 orbits shown here. Compare with Fig. 8 which shows the evolution of the same variables for an intermediate friction time run.

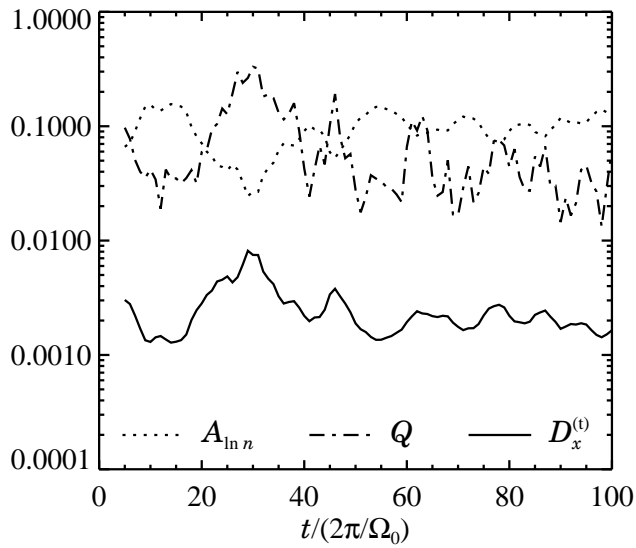


Fig. 8.— Same as Fig. 7, but for the intermediate friction time run 64c.x. Obviously the cosine amplitude and the derived turbulent diffusion coefficient change much more violently with time. The fit quality is also a lot worse. The average diffusion coefficient is actually the same as for the short friction time run shown in Fig. 7, but the poor fit quality here means that the diffusion description of turbulent transport is not as good as it is in the short friction time runs.

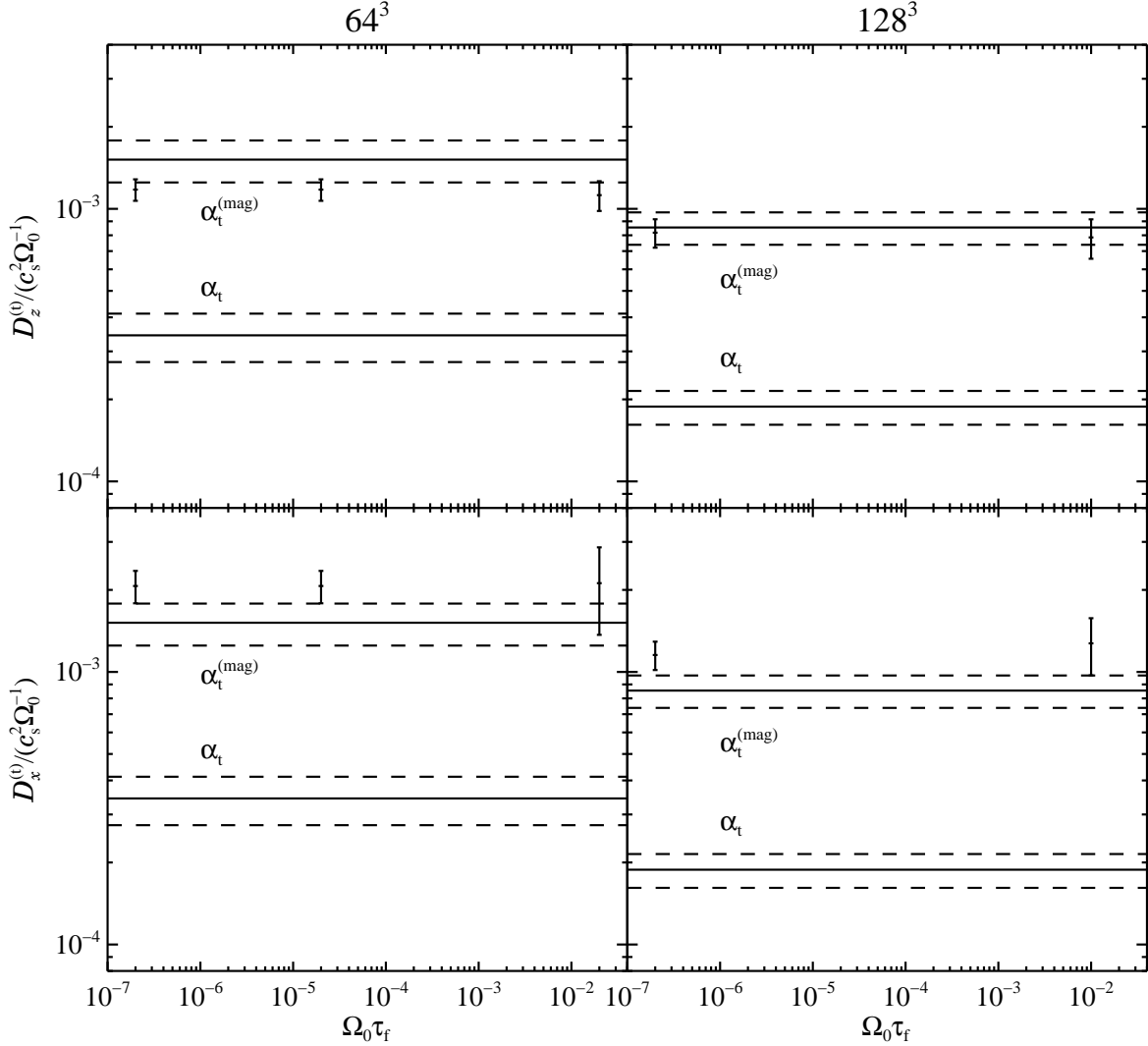


Fig. 9.— The measured turbulent diffusion coefficient as a function of $\Omega_0 \tau_f$ for a resolution of 64^3 (left panels) and 128^3 (right panels). The vertical diffusion coefficient is shown in the top panels, while the radial diffusion coefficient is shown in the bottom panels. For reference the turbulent α -values based on both the Reynolds stress and the Maxwell stress are shown including their $1\text{-}\sigma$ fluctuation intervals. The radial diffusion coefficient is comparable to the sum of the turbulent α -values and is around 70% higher than the vertical diffusion coefficient.

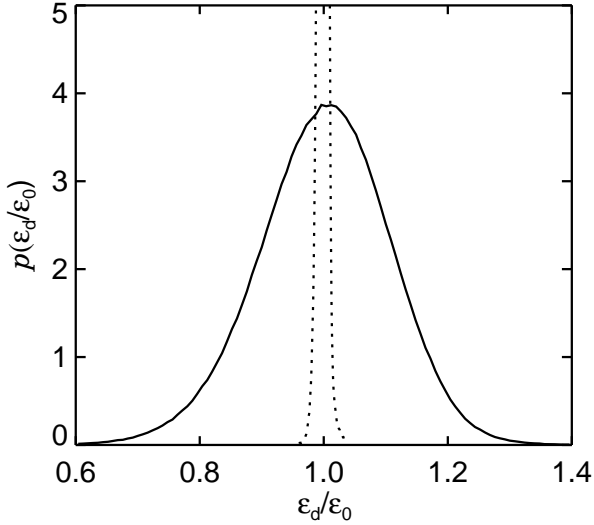


Fig. 10.— Dust-to-gas ratio probability distribution function for runs with $\Omega_0\tau_f = 0.02$ (full line) and $\Omega_0\tau_f = 2 \times 10^{-7}$ (dotted line) without gravity on the dust. For the intermediate friction run, there is a much higher probability for very low or very high dust-to-gas ratios, compared to the short friction time run where the dust-to-gas ratio is sharply peaked around $\epsilon_d = \epsilon_0$. The full probability curve for the short friction time run is shown in Fig. 11.

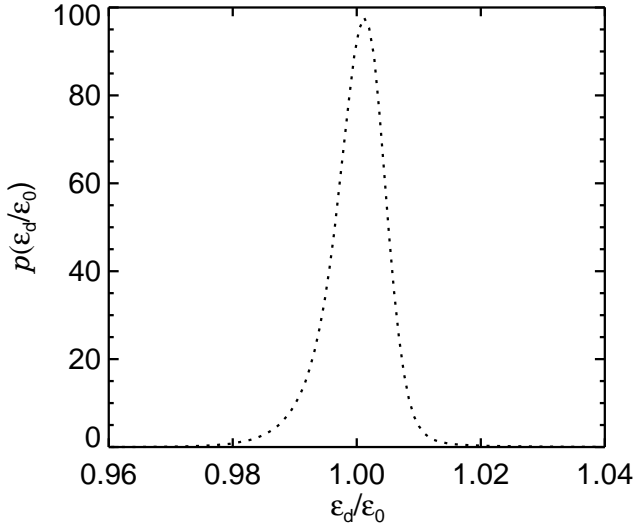


Fig. 11.— The full dust-to-gas ratio probability distribution function for a short friction time run with $\Omega_0\tau_f = 2 \times 10^{-7}$ and no gravity. Because the peak is so sharp compared to the intermediate friction time run, only the lower part is shown in Fig. 10.

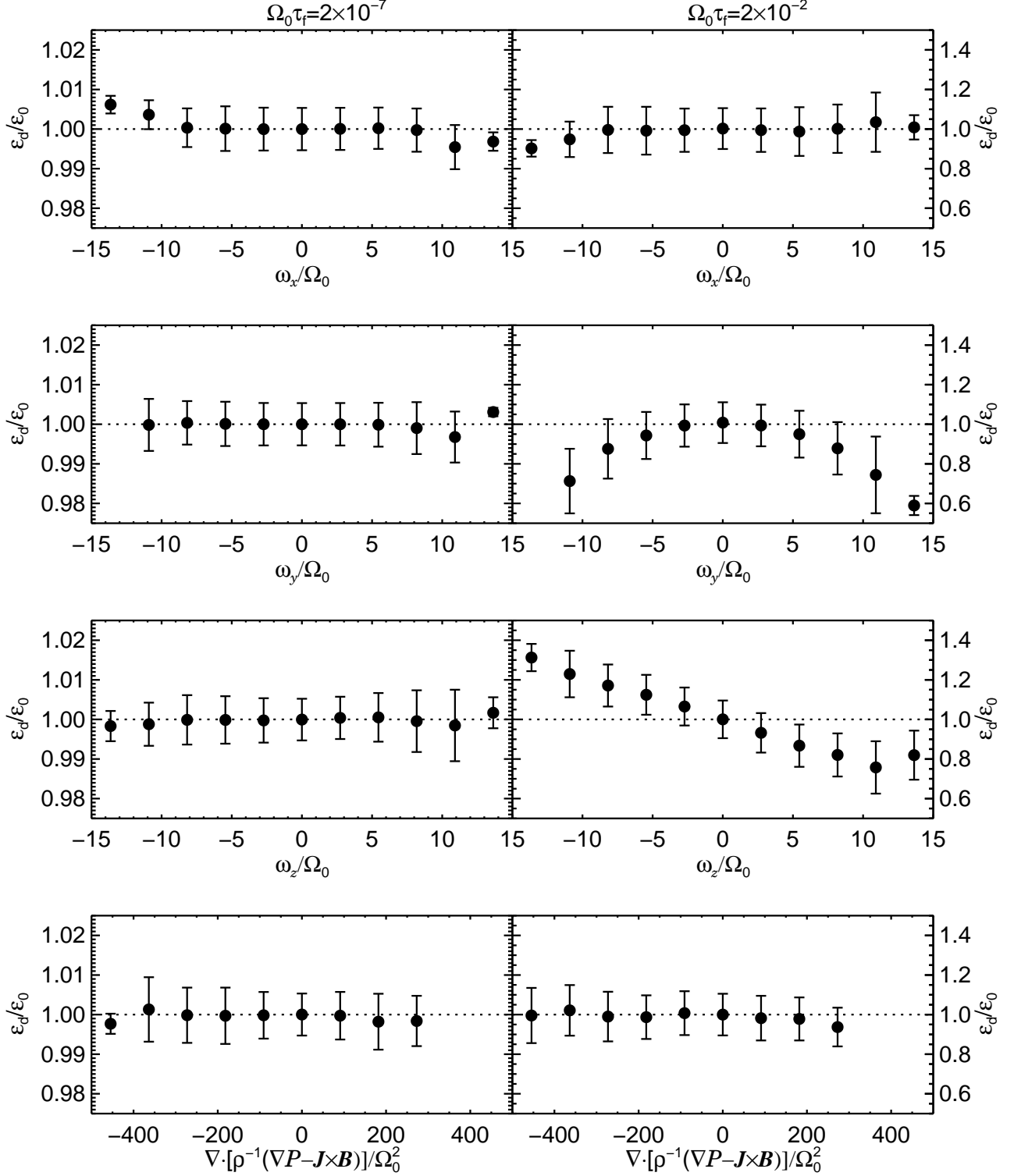


Fig. 12.— The dust-to-gas ratio ϵ_d in bins of vorticity components (first three rows) and divergence of pressure gradient flux (last row). The large dot shows the average dust-to-gas ratio in the bin, while the bars represent the fluctuation interval. The clearest correlation is between vertical vorticity and dust-to-gas ratio for the intermediate friction time run. This may be due to vortex trapping as explained in the text.

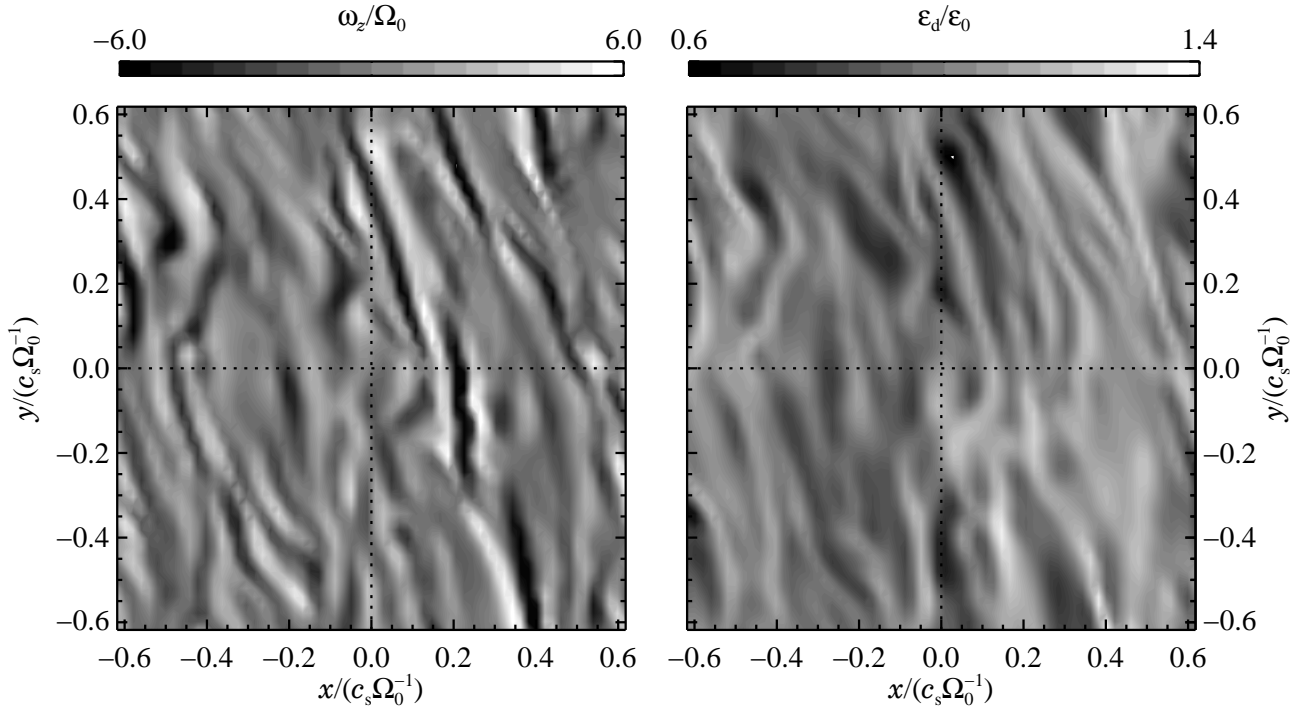


Fig. 13.— Contour plots of vertical component of vorticity (left panel) and dust-to-gas ratio (right panel) in an arbitrary z -plane for the intermediate friction time run 64c_ng. There is a tendency for positive vorticity (light regions) to correspond to low dust-to-gas ratio (dark regions) and vice versa. This indicates that dust grains are being trapped in turbulent eddies by the vortex trapping mechanism. The dotted lines are reference lines to make comparison between the two plots easier.

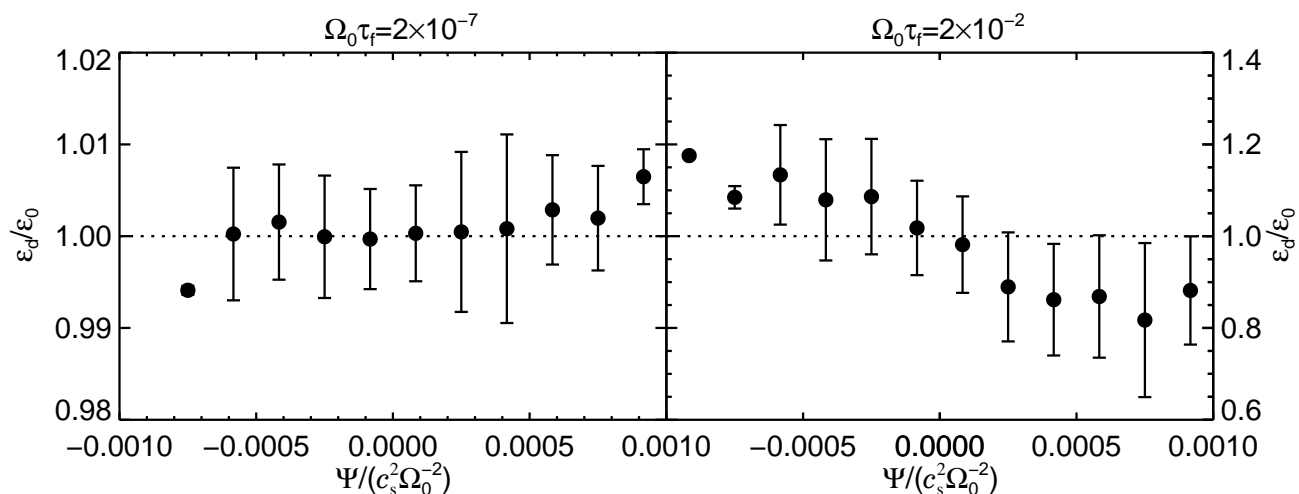


Fig. 14.— Plot of dust-to-gas ratio in bins of vortex parameter $\Psi \equiv [-(\mathbf{u} \cdot \nabla)\mathbf{u}] \cdot \mathbf{f}(\mathbf{u})$. Anticyclonic vortices have a negative value of Ψ , whereas for cyclonic vortices Ψ is positive. For the intermediate friction time run, there is a clear anticorrelation between vortex parameter and dust-to-gas ratio. This is an indication that dust is being trapped in anticyclonic vortices.

Table 1. Run parameters

Run	Res	$g_z^{(0)}$	$g_x^{(0)}$	$\Omega_0 \tau_f$	a_{\bullet}/m	SFTA	$\mu_3 = \eta_3 = D_3$
64a _z	64 ³	1000	0	2×10^{-7}	2×10^{-7}	Yes	1.3×10^{-11}
64b _z	64 ³	10	0	2×10^{-5}	2×10^{-5}	Yes	1.3×10^{-11}
64c _z	64 ³	0.01	0	0.02	0.02	No	1.3×10^{-11}
128a _z	128 ³	1000	0	2×10^{-7}	2×10^{-7}	Yes	1.3×10^{-12}
128c _z	128 ³	0.01	0	0.01	0.01	No	1.3×10^{-12}
64a _x	64 ³	0	1000	2×10^{-7}	2×10^{-7}	Yes	1.3×10^{-11}
64b _x	64 ³	0	10	2×10^{-5}	2×10^{-5}	Yes	1.3×10^{-11}
64c _x	64 ³	0	0.01	0.02	0.02	No	1.3×10^{-11}
128a _x	128 ³	0	1000	2×10^{-7}	2×10^{-7}	Yes	1.3×10^{-12}
128c _x	128 ³	0	0.01	0.01	0.01	No	1.3×10^{-12}
64a _{ng}	64 ³	0	0	2×10^{-7}	2×10^{-7}	Yes	1.3×10^{-11}
64c _{ng}	64 ³	0	0	0.02	0.02	No	1.3×10^{-11}

Note. — The first column gives the name of the run, the second the resolution, the third and fourth the vertical and radial gravity strength, the fifth column the friction time, the sixth column the corresponding grain radius in a typical solar nebula at $r_0 = 5$ AU, the seventh column whether we used the short friction time approximation or not, and the eighth column the value of the artificial viscosity μ_3 , magnetic diffusivity η_3 and mass diffusion D_3 .

Table 2. Turbulent viscosities and turbulent diffusion coefficients

Run	$\alpha_t/10^{-3}$	$\alpha_t^{(\text{mag})}/10^{-3}$	$D_z^{(t)}/10^{-3}$	$D_x^{(t)}/10^{-3}$	Pd_z	Pd_x
64a_z	0.34 ± 0.07	1.52 ± 0.27	1.18 ± 0.11	—	1.58	—
64b_z	0.34 ± 0.07	1.52 ± 0.27	1.18 ± 0.11	—	1.58	—
64c_z	0.33 ± 0.08	1.47 ± 0.29	1.12 ± 0.14	—	1.60	—
64a_x	0.34 ± 0.07	1.52 ± 0.27	—	2.07 ± 0.28	—	0.90
64b_x	0.34 ± 0.07	1.52 ± 0.27	—	2.07 ± 0.28	—	0.90
64c_x	0.33 ± 0.08	1.47 ± 0.29	—	2.12 ± 0.75	—	0.85
128a_z	0.19 ± 0.03	0.85 ± 0.12	0.82 ± 0.10	—	1.27	—
128c_z	0.19 ± 0.04	0.85 ± 0.19	0.79 ± 0.13	—	1.31	—
128a_x	0.16 ± 0.02	0.75 ± 0.10	—	1.15 ± 0.14	—	0.79
128c_x	0.18 ± 0.03	0.83 ± 0.12	—	1.27 ± 0.30	—	0.79

Note. — The first column gives the name of the run. The second and third columns show the turbulent α -values based on Reynolds and Maxwell stresses, respectively. Since there is no back-reaction from the dust on the gas, these values are only affected by the dust through the dust’s contribution to the time-step. The next two columns show the measured turbulent diffusion coefficients, and in the last two columns we write the vertical and radial turbulent diffusion Prandtl numbers.